1 **The formation of a camalexin-biosynthetic metabolon**

2

3 Stefanie Mucha[a,b], Stephanie Heinzlmeir[c], Verena Kriechbaumer[d], Benjamin
4 Strickland[a], Charlotte Kirchhelle[b, 2], Manisha Choudhary[b], Natalie Kowalski[a], Ruth
5 Eichmann[e, 3], Ralph Hückelhoven[e], Erwin Grill[a], Bernhard Küster[c], Erich
6 Glawischnig[a, b, f, 1]

7 [a] Chair of Botany, Department of Plant Sciences, Technical University of Munich,
8 Emil-Ramann-Str. 4, 85354 Freising, Germany.
9 [b] Chair of Genetics, Department of Plant Sciences, Technical University of Munich,
10 Emil-Ramann-Str. 8, 85354 Freising, Germany.
11 [c] Chair of Proteomics and Bioanalytics, Technical University of Munich, Emil-
12 Erlenmeyer-Forum 5, 85354 Freising, Germany.
13 [d] Plant Cell Biology, Biological and Medical Sciences, Oxford Brookes University,
14 Oxford, OX3 0BP, UK.
15 [e] Chair of Phytopathology, Department of Plant Sciences, Technical University of
16 Munich, Emil-Ramann-Str. 2, 85354 Freising, Germany.
17 [f] Microbial Biotechnology, TUM Campus Straubing for Biotechnology and
18 Sustainability, Technical University of Munich, Schulgasse 22, 94315 Straubing,
19 Germany (present address).

20 [1] corresponding author, Email: Glawischnig@tum.de.
21 [2] present address: Department of Plant Sciences, University of Oxford, South Parks
22 Road, Oxford OX1 3RB, UK

23 [3] present address: School of Life Sciences, University of Warwick, Gibbet Hill
24 Campus, Coventry, CV4 7AL, UK

25 ORCID IDs: 0000-0002-6382-7035 (S.M.); 0000-0002-1066-6565 (S.H.); 0000-0003-
26 3782-5834 (V.K.); 0000-0002-1387-9013 (B.S.); 0000-0001-8448-6906 (C.K.); 0000-
27 0001-8158-1318 (M.C.); 0000-0002-9464-6456 (N.K.); 0000-0002-9307-7773 (R.E.);
28 0000-0001-5632-5451 (R. H.); 0000-0003-4036-766X (E. Gr.); 0000-0002-9094-1677
29 (B.K.); 0000-0001-9280-5065 (E.Gl.)

30

31 Short title: The camalexin-biosynthetic metabolon

32

33

34 One-sentence summary: In *Arabidopsis thaliana*, the cytochrome P450 enzymes of
35 the camalexin biosynthetic pathway form a metabolic complex to which the
36 glutathione transferase U4 is recruited.

37

41
42
43 **Abstract**
44

45 *Arabidopsis thaliana* efficiently synthesizes the antifungal phytoalexin camalexin
46 without apparent release of bioactive intermediates, such as indole-3-acetaldoxime,
47 suggesting channeling of the biosynthetic pathway by formation of an enzyme
48 complex. To identify such protein interactions, two independent untargeted co-
49 immunoprecipitation (co-IP) approaches with the biosynthetic enzymes CYP71B15
50 and CYP71A13 as baits were performed and the camalexin biosynthetic P450
51 enzymes were shown to co-purify. These interactions were confirmed by targeted co-
52 IP and Förster resonance energy transfer measurements based on fluorescence
53 lifetime microscopy (FRET-FLIM). Furthermore, interaction of CYP71A13 and
54 Arabidopsis P450 Reductase 1 (ATR1) was observed. An increased substrate affinity
55 of CYP79B2 in presence of CYP71A13 was shown, indicating allosteric interaction.
56 Camalexin biosynthesis involves glutathionylation of an intermediary indole-3-
57 cyanohydrin, synthesized by CYP71A12 and especially CYP71A13. It was
58 demonstrated by FRET-FLIM and co-IP, that the glutathione transferase GSTU4,
59 which is co-expressed with tryptophan- and camalexin-specific enzymes, was
60 physically recruited to the complex. Surprisingly, camalexin concentrations were
61 elevated in knock-out and reduced in *GSTU4* overexpressing plants. This shows that
62 GSTU4 is not directly involved in camalexin biosynthesis but rather has a role in a
63 competing mechanism.

64

65 **Introduction**

66 Cytochrome P450 enzymes are found in all domains of life, but are particularly
67 diversified in plants. In *Arabidopsis thaliana*, 244 P450-encoding genes are
68 annotated, and individual enzymes have been shown to play roles e.g. in the

2

biosynthesis of phytohormones or of compounds involved in defense (Bak et al., 2011). However, the biological function of the vast majority of Arabidopsis P450 enzymes remains unclear. Typically, eukaryotic P450 enzymes are anchored to the membrane of the endoplasmic reticulum (ER) with their catalytic centers facing the cytosolic side. They are able to form homo- and heteromers (Reed and Backes, 2012) and there is growing evidence that these interactions have an effect on the catalytic activities of the respective enzymes. This has been shown in detail for the human enzymes CYP2E1, CYP3A4, and CYP3A5 (Davydov et al., 2015).

In contrast to human/animal systems, for plant P450 enzymes there is little information on potential functional interactions. For CYP73A5 and CYP98A3, physical interactions with each other and additional enzymes of the phenylpropanoid biosynthetic pathway was demonstrated by co-purification and Förster resonance energy transfer (FRET) (Bassard et al., 2012). Also for sporopollenin biosynthesis, involving CYP703 and CYP704 isoforms, interactions with other pathway enzymes have been demonstrated by pulldown, yeast-2-hybrid and FRET experiments (Lallemand et al., 2013). Furthermore, there is evidence for complex formation of flavonoid biosynthetic enzymes (Crosby et al., 2011; Dastmalchi et al., 2016). Recently, it was shown in detail that the cyanogenic glucoside Dhurrin is synthesized by a protein complex of two cytochrome P450 enzymes, a P450 reductase and a glucosyl transferase (Laursen et al., 2016). These examples indicate formation of transient enzyme complexes, also referred to as metabolons, allowing efficient channeling of intermediates, in particular for the biosynthesis of secondary metabolites (Fujino et al., 2018; Hawes and Kriechbaumer, 2018; Knudsen et al., 2018).

In Arabidopsis, cytochrome P450 enzymes play a crucial role in the biosynthesis of indolic defense compounds, such as indole glucosinolates, camalexin, 4-hydroxyindole-3-carbonyl nitrile, or derivatives of indole-3-carboxylic acid (Rauhut and Glawischnig, 2009; Sønderby et al., 2010; Böttcher et al., 2014; Rajniak et al., 2015) (Fig. 1). For the biosynthesis of these specialized metabolites, tryptophan is converted to indole-3-acetaldoxime (IAOx) by CYP79B2 and CYP79B3. *Cyp79b2 cyp79b3* double mutants, in which tryptophan-derived defense compounds are essentially absent, have been shown to be significantly more susceptible to a variety of pathogens (Zhao et al., 2002; Glawischnig et al., 2004; Böttcher et al., 2009; Schlaeppi et al., 2010; Frerigmann et al., 2016). In healthy plants, IAOx is

103   predominantly oxidized by CYP83B1 (SUR2, RNT1) to the corresponding nitrile
104   oxides or *aci*-nitro compound (Bak et al., 2001; Hansen et al., 2001), the precursors
105   of indole glucosinolates. Pathogen infection or treatment with high dosages of UV
106   light or heavy metals, such as silver nitrate, induce the production of CYP71A12 and
107   CYP71A13, which in contrast dehydrate IAOx to indole-3-acetonitrile (IAN) in the
108   biosynthesis of camalexin (Nafisi et al., 2007; Müller et al., 2015), which is the major
109   metabolite synthesized in response to these stresses. In camalexin biosynthesis, IAN
110   is then activated, presumably to indole cyanohydrin, which also involves CYP71A12
111   and CY71A13, and conjugated with glutathione (Parisy et al., 2007) yielding GS-IAN.
112   Glutathionylations are catalyzed by glutathione transferases (GSTs), which are found
113   in all eukaryotes. Arabidopsis contains 54 *GST* genes belonging to 7 different classes
114   (Krajewski et al., 2013). A number of GSTs have been shown to be capable of
115   metabolizing xenobiotics (Dixon et al., 2002; Wagner et al., 2002), but with a few
116   exceptions (Kitamura et al., 2004) the information on endogenous functions is limited,
117   and it is unclear to which degree they are functionally redundant (Czerniawski and
118   Bednarek, 2018). For GS-IAN formation, Su et al. (2011) suggested an involvement
119   of GSTF6, which is a member of a small subfamily together with GSTF2, GSTF3 and
120   GSTF7. Interestingly, camalexin concentrations detected in response to silver nitrate
121   were not significantly different with respect to wildtype even in *gstf2 gstf3 gstf6* triple
122   knockout mutants or a *gstf2 gstf3 gstf6 gstf7* knockdown line (Rauhut, 2009). This
123   shows that alternative GSTs might also participate in this step. Subsequently, GS-
124   IAN is shortened to Cys(IAN) involving gamma-glutamyl peptidase 1 (GGP1), and
125   Cys(IAN) is then converted to camalexin by a unique bifunctional P450 enzyme,
126   CYP71B15 (Fig. 1). *Cyp71b15* mutants (*phytoalexin deficient 3*, *pad3*) are camalexin-
127   deficient and accumulate camalexin precursors, such as Cys(IAN), dihydrocamalexic
128   acid (DHCA) and derivatives thereof (Glazebrook and Ausubel, 1994; Zhou et al.,
129   1999; Bednarek et al., 2005; Schuhegger et al., 2006; Böttcher et al., 2009).

130   Despite camalexin being a major sink for tryptophan in response to various stresses,
131   intermediates such as IAOx are not accumulating, suggesting possible metabolite
132   channeling between interacting proteins. Therefore, we have hypothesized that
133   camalexin is produced by a metabolon. In this work, we provide evidence that the
134   cytochrome P450 enzymes of the camalexin biosynthetic pathway physically interact
135   and we systematically analyzed the potential functions of GSTs in camalexin
136   formation.

4

Results

Cellular and subcellular localization of CYP71B15

CYP71B15 was expressed as C-terminal GFP fusion protein under control of its own promoter. This construct was expressed in a *pad3* knockout mutant background and lines complementing the camalexin-deficient phenotype were selected. Expression of the CYP71B15-GFP protein was monitored by Western blot analysis and a line was selected for further analysis in which a strong GFP signal was observed in response to *Botrytis cinerea* infection, while the signal was absent in untreated leaves (Supplemental Figure 1A).

As a next step, we analyzed the cellular distribution and subcellular localization of CYP71B15-GFP in response to the fungal pathogens *B. cinerea, Alternaria brassicicola,* and *Erysiphe cruciferarum* (Fig. 2). In accordance with its biological function in phytoalexin biosynthesis, CYP71B15-GFP was only observed in cells in close proximity to successful pathogen infection. We observed a strong accumulation of CYP71B15-GFP around the site to *B. cinerea* infection (24 h after infection, hai) (Fig 2A-F), surrounding an area, where the necrotrophic fungus had apparently already started to macerate the leaf tissue and where no CYP71B15-GFP was detected, possibly because these cells were no longer metabolically active. For necrotrophic *A. brassicicola* (18 hai), CYP71B15-GFP expression, was only observed in cells in direct cellular contact with the fungus (Fig. 2G-L). In *E. cruciferarum* infected leaves (24 hai), highest CYP71B15-GFP abundance was observed in cells next to cells that had been attacked or penetrated by the biotrophic fungus (Fig. 2 M-R). Note that *E. cruciferarum* spores, which were not germinated, did not induce CYP71B15-GFP expression (Fig 2M-O). In all cases, CYP71B15-GFP was located in the ER, which also surrounds the nucleus. This is in accordance with the detected ER-localization in the heterologous *Nicotiana* system (see below). No focal protein accumulations at sites of plant-microbe interactions were detected.

Untargeted screen for interaction partners of CYP71B15

Applying this *CYP71B15_{pro}:CYP71B15-GFP* (*pad3*) line, an untargeted proteomics screen was set up to identify proteins which interact with CYP71B15 in *B. cinerea-*

infected, as model system for pathogen interactions, or in UV-irradiated plants. Rosette leaves of six weeks-old *CYP71B15pro:CYP71B15-GFP* (*pad3*) and *pad3* plants were infected with *B. cinerea*. After 24 h, microsomes were prepared and solubilized. Co-IPs were performed and the eluates were subjected to trypsin digestion and MS analysis. An aliquot of starting material was also analyzed to determine the composition of microsomal proteins in response to *B. cinerea* infection. Along with the bait protein CYP71B15, which was the protein corresponding to the highest signal intensity, a total of 71 proteins significantly accumulated with respect to the control IPs. Strikingly, among these, 22 cytochrome P450 enzymes, *e.g.* CYP71B23, CYP84A1, and CYP706A1, were highly overrepresented (Fig. 3; Supplemental Figure 2A). CYP71A13, the enzyme channeling IAOx into the camalexin biosynthetic pathway, was among the interacting proteins which accumulated with highest intensity (average $\log_2$ intensity = 25.4) and highest specificity (109-fold enrichment, p=0.00014). Interestingly, the P450 enzyme CYP83B1 which competes with camalexin-specific enzymes for the intermediate IAOx (Fig. 1) (Bak et al., 2001; Hansen et al., 2001), and CYP71B6 which is involved in IAN metabolism (Bak et al., 2001; Hansen et al., 2001; Böttcher et al., 2014; Müller et al., 2019), were also enriched. CYP71A12 was also significantly enriched with an Label-free quantification (LFQ) intensity approx. 12-fold lower than CYP71A13. CYP79B2 and ATR1 were detected in the co-IP, but the respective enrichments (4.5-fold, p=0.17 and 5.0-fold, p=0.022, respectively) were below the threshold of significance indicating weak or transient interaction with the observed CYP71B15-containing protein complex. Interestingly, PDR12/ABCG40, which was recently identified as camalexin transporter (He et al., 2019) was significantly enriched (7.8-fold; p=0.00029), indicating that biosynthesis and transport of camalexin to some extent might be physically linked. For a comprehensive overview of the proteomics data, see Supplemental Dataset 1.

To evaluate to which extent this result depends on the trigger of camalexin biosynthesis, IPs were also performed with UV-irradiated leaves. The general outcome was similar (Supplemental Figure 2B): Besides the bait, which showed highest abundance, P450 enzymes such as CYP71A13, CYP83B1 and CYP71B6 were highly enriched, but also CYP79B2 and CYP71A12 were co-purified with CYP71B15 (Supplemental Dataset 1).

Screen for inducible physical interactors of CYP71A13

CYP71A13 was consistently identified as interactor in an untargeted screen with CYP71B15 as bait. As a complementary approach, a CYP71A13-YFP fusion protein was expressed in Arabidopsis under control of the 35S promoter. Microsomes of UV-irradiated or untreated rosette leaves were isolated and solubilized, and a co-IP was performed to address (i) whether CYP71B15-CYP71A13 interaction is independent of the choice of baits, and (ii) which interaction partners specifically bind CYP71A13 in response to induction. A total of 875 proteins were reproducibly detected in the co-IPs of the UV-treated samples (Supplemental Dataset 2), including 26 cytochrome P450 enzymes, and the cytochrome P450 reductases ATR1 and ATR2. Constitutive expression of the bait allows to detect also binding partners under control conditions, where concentrations of CYP71A13 expressed under control of its native promoter are too low for quantitative work. As this approach can yield also unspecific binding partners, the analysis was focused on the differences of UV treatment versus control. Strikingly, only one protein, CYP71B15, was significantly enriched in the UV-treated versus the non-treated sample (Fig. 4). Five proteins were significantly depleted in the UV-treated versus the non-treated sample, including Nitrilase 3 (NIT3, approx. 7-fold), which has been suggested to convert IAN to the auxin indole-3-acetic acid (IAA) upon sulphur starvation (Kutz et al., 2002).

In summary, we conclude from the untargeted co-IP experiments that the core camalexin biosynthetic enzymes CYP71B15 and CYP71A13 physically interact with each other in challenged Arabidopsis rosette leaves. Also, CYP71B6 which specifically converts IAN to Indole-3-aldehyde (ICHO) and Indole-3-carboxylic acid (ICOOH) (Böttcher et al., 2014) was consistently identified as a member of the protein complex. In the untargeted screens, CYP79B2 was identified as binding partner of CYP71B15, although the specificity of this interaction was not significant. No interaction in an untargeted screen with CYP71A13 was observed. This indicates that binding of CYP79B2 to the proposed camalexin biosynthetic protein complex is weaker and more transient than the interaction between the camalexin-specific enzymes CYP71A13 and CYP71B15.

Physical interaction of camalexin biosynthetic enzymes is confirmed by targeted co-IP

236   In order to confirm the physical interaction of the camalexin biosynthetic enzymes
237   CYP71A12, CYP71A13, CYP71B15 and ATR1, different combinations of these
238   proteins were transiently expressed in *Nicotiana benthamiana* as C-terminally YFP-
239   and FLAG-tagged proteins. Solubilized microsomes were applied to α-GFP-beads
240   and IP and co-IP was monitored by Western Blot with GFP- and FLAG-specific
241   antibodies, respectively (Fig. 5; Supplemental Figure 3). As negative controls, all
242   proteins were additionally co-expressed with membrane-bound GFP in order to
243   exclude protein interaction due to the YFP tag or unspecific binding of the FLAG
244   tagged proteins to the polysaccharide chains of the GFP trap beads used for targeted
245   co-IP. Interaction was shown for CYP71A13 with CYP71B15 and ATR1. CYP71B15
246   also interacts with CYP71A12. In addition, interaction of CYP71A13 and CYP71B15
247   with the glutathione transferase (GST) U4 (see below) was observed.

248

249   **CLSM microscopy and FRET-FLIM analysis demonstrate physical interaction of**
250   **biosynthetic enzymes *in vivo***

251   The subcellular localization of CYP71A12, CYP71A13, CYP71B15 and CYP79B2, as
252   well as of GGP1 and the GSTs U2 and U4 (Fig. 6), was analyzed by confocal
253   microscopy, three days after transient expression of corresponding C-terminal GFP-
254   and RFP-fusion proteins in *N. benthamiana* (Fig. 6, Supplemental Figure 4).
255   CYP71A12 (Supplemental Fig. 4A), CYP71A13 (Supplemental Fig. 4B), and
256   CYP71B15 (Supplemental Fig. 4C) were localized to the ER and showed co-
257   localization with the ER lumenal marker RFP-HDEL and with each other (Fig. 6 A-C,
258   D-F). Interestingly, although all experimental conditions were chosen identical to the
259   other P450 enzymes analyzed, CYP79B2-RFP expression was always weaker (Fig.
260   6G). Nevertheless, co-localization with CYP71A13 was observed (Fig. 6 I).
261   Apparently, GGP1 was localized to the cytosol and to some extent mis-localization of
262   CYP71A13 to the cytoplasm was induced by GGP1 co-expression (Fig. 6 J-L).

263   We analyzed physical interaction by FRET (Förster, 1948) measured by donor
264   excited-state FLIM (Becker, 2012; Schoberer and Botchway, 2014). The reduction in
265   the lifetime of the GFP (donor) fluorescence occurs only when an acceptor
266   fluorophore (mRFP) is within a distance of 10 nm, indicating a very high proximity
267   and most likely direct physical contact between the two proteins of interest.
268   Fluorescence lifetime of CYP71A12-GFP (Fig. 7A), CYP71A13-GFP (Fig. 7B), and

269 CYP71B15-GFP (Fig. 7C) was quantified in combination with various potential
270 binding partners. Interaction was shown for CYP71A12 with CYP71B15, CYP79B2,
271 GSTU4 and the soluble camalexin-biosynthetic enzyme GGP1. CYP71A13 binds to
272 CYP71A12, CYP71B15, CYP79B2, GSTU4, and GGP1. Furthermore, the
273 fluorescence lifetime of CYP71B15-GFP in presence of CYP71A12, CYP79B2,
274 GSTU4 or GGP1 was statistically significantly reduced, which indicates an interaction
275 of also these enzymes.

276 Taking the co-IP and FRET-FLIM data together, essentially it was demonstrated that
277 the known camalexin biosynthetic enzymes form a protein complex *in vivo*.
278 Interestingly, no CYP71A12 or CYP71B15 homodimer formation was observed. This
279 also demonstrates that e.g. the observed interactions between CYP71A12/A13 and
280 CYP71B15 are not due to unspecific dimerization of the cytochrome P450s.

281

Enzymatic parameters of CYP79B2 indicate allosteric interaction with
CYP71A13

284 In order to examine potential metabolic channeling, the first two pathway enzymes,
285 CYP79B2 and CYP71A13 were co-expressed together with ATR1 in *Saccharomyces*
286 *cerevisiae*. As a control, the CYP71A13 expression construct was replaced by an
287 empty vector. Tryptophan-conversion by corresponding microsomes was monitored.
288 A striking shift of the product spectrum towards formation of IAN was observed for
289 CYP79B2/CYP71A13, with respect to CYP79B2/empty vector microsomes (Fig. 8A).
290 In addition, co-expression of CYP79B2 and CYP71A13 reduced the apparent Km-
291 value of CYP79B2 for tryptophan more than two-fold (6.9 ± 0.9 µM versus 17.5 ± 1.9
292 µM) (Fig. 8B).

293

GSTU4 physically interacts with CYP71A13 and is relevant for the camalexin
response

296 In camalexin biosynthesis, activated IAN, presumably indole cyanohydrin, is
297 glutathionylated, probably involving a GST (Klein et al., 2013). The untargeted co-IP
298 screens (Supplemental datasets 1 and 2) revealed only few GSTs as proteins co-
299 purified with very low signal intensity. GSTF6, previously proposed to be involved in
300 camalexin biosynthesis (Su et al., 2011) was not detected. Possibly the interaction of

301   the cytosolic GSTs with the P450 enzymes is not sufficiently strong to persist in
302   presence of the applied Triton X-100 concentration. To evaluate which Arabidopsis
303   GSTs are capable of this conversion, a qualitative screening was performed in a
304   yeast strain in which four endogenous GSTs and three genes of glutathione
305   conjugate catabolism were deleted (GTO1, GTO2, GTO3, TEF4, CPC, CPY, CIS2)
306   (Krajewski et al., 2013; Kowalski, 2016) and in which expression plasmids for ATR1
307   and CYP71A13 were introduced. These yeast cells were transformed with each of
308   the 54 Arabidopsis GSTs and after selection screened for biotransformation of IAN
309   and glutathione yielding GS-IAN. When an empty vector was used instead of the
310   CYP71A13 expression plasmid, no activity was detected. Also, when no Arabidopsis
311   GST was expressed, no GS-IAN was synthesized. Strikingly, for 41 enzymes,
312   including most of the phi- and tau-class GSTs, product formation was observed
313   (Supplemental Figure 5). As an approach to identify which of the active GSTs is
314   relevant *in planta*, transcriptomics data was surveyed for co-expression with
315   camalexin biosynthetic genes. In particular, *GSTU4* is strongly induced by pathogens
316   and correlated with the genes of camalexin biosynthesis (CYP71B15, r=0.85;
317   CYP71A13 r=0.77, expression angler, *B. cinerea* set (Toufighi et al., 2005), see also
318   Supplemental Table 1).

319   GSTU4 was co-expressed with CYP71A13 in *N. benthamiana* as RFP/GFP fusion
320   proteins and their subcellular localization was monitored (Fig. 6; Supplemental Figure
321   4, 6). As control, GSTU2 was included, which is closely related to GSTU4 and a
322   member of the same gene cluster, and only weakly transcriptionally co-regulated with
323   genes of camalexin biosynthesis (CYP71B15, r=0.53, CYP71A13, r=0.62, expression
324   angler (Toufighi et al., 2005), *B. cinerea* set). Physical interaction was tested for both
325   pairs by FRET-FLIM. For GSTU4-RFP a strong reduction of the CYP71A12-GFP,
326   CYP71A13-GFP and CYP71B15-GFP lifetimes was detected (Fig. 7). All three
327   CYP71s and GSTU2 did not physically interact (Fig. 7). Interaction of GSTU4 with
328   CYP71A13 and CYP71B15 was also demonstrated via co-IP analysis (Fig. 5)

329   To evaluate a potential function of GSTU2 and GSTU4 in camalexin biosynthesis,
330   *gstu2* and *gstu4* knockout as well as *GSTU4* overexpression lines were analyzed for
331   camalexin formation in response to UV-C light (Supplemental Figure 7A), silver
332   nitrate treatment (Supplemental Figure 7B) and *B. cinerea* infection (Supplemental
333   Figure 7C). While for *gstu2* no difference in camalexin levels relative to a wild-type
334   control was observed, *gstu4* knockout mutants typically showed elevated camalexin

335   concentrations. Strikingly, in response to *B. cinerea* infection, *35S~pro~:GSTU4*

336   overexpression lines accumulated less camalexin than wildtype plants. To statistically

337   evaluate these effects, data from four independent experiments were combined (Fig.

338   9). There is a significant negative effect of *GSTU4* on the relative camalexin

339   concentration accumulating in response to *B. cinerea* infection.

340

Discussion

342   The physical interaction of enzymes is a powerful strategy to effectively channel

343   biosynthetic pathways and avoid release of reactive intermediates. Upon induction,

344   camalexin is a major sink for tryptophan. Nevertheless, intermediates such as IAOx

345   are not accumulating, indicating metabolite channeling. Camalexin biosynthesis

346   involves several P450 enzymes which are bound to ER membranes. Membrane

347   anchoring restricts diffusion facilitating that P450 enzymes can serve as nuclei for the

348   formation of metabolic complexes. In addition, the ER membrane can reorganize

349   bringing cytochrome P450 enzymes into contact with pathway enzymes in other

350   organelles, which was *e.g.* observed for CYP81F2 in the interaction of Arabidopsis

351   with nonadapted powdery mildew *Blumeria graminis f. sp hordei* (*Bgh*)(Fuchs et al.,

352   2016). For the ultimate enzyme of the camalexin biosynthetic pathway, CYP71B15

353   (PAD3), in the interaction with *B. cinerea, A. brassicicola,* and *E. cruciferarum* (Fig. 2)

354   we observed a strong induction of protein expression, but no focal accumulation.

355   Highly localized expression at sites of interaction together with metabolic channeling

356   in multienzyme complexes may ensure highly controlled and safe production of

357   camalexin on demand.

358   We identified proteins which physically interact with CYP71B15 (PAD3) following an

359   untargeted co-IP approach (Fig. 3). The relative abundance of the co-purified

360   proteins do not reflect the relative protein abundance of the corresponding solubilized

361   microsomes, which served as starting material. Based on LFQ intensities, P450

362   enzymes represent only a minor fraction of total microsomal proteins, whilst they are

363   highly overrepresented in the co-IP samples and highly enriched with respect to

364   control IPs. This shows that the interaction between CYP71B15 and other P450

365   enzymes is not random. CYP71A12 and CYP71A13 were co-purified with high

366   significance, demonstrating the specific interaction of camalexin biosynthetic

367 enzymes. In addition, enzymes involved in other pathways, such as phenylpropanoid
368 or glucosinolate metabolism, were also significantly enriched, including CYP71B6,
369 which degrades IAN to ICOOH and cyanide. Remarkably, the detected CYP71B15-
370 CYP73A5 and CYP71B15-CYP98A3 interactions were also observed in a reverse
371 approach with the two phenylpropanoid biosynthetic enzymes as baits in a tandem
372 affinity purification-based screen (Bassard et al., 2012). Possibly, direct or indirect
373 interactions of CYP71B15 with P450 enzymes of other biosynthetic pathways involve
374 mutual regulation of their catalytic activities. Alternatively, ER-bound P450s tend to
375 interact as they are dependent on the reductases ATR1 or ATR2 (Bassard et al.,
376 2012). However, these P450 reductases were detected in solubilized microsomes but
377 not significantly enriched by co-IP. In addition, a number of membrane-bound kinases
378 were enriched. Whether this interaction has a functional significance, e.g. by
379 phosphorylation of the biosynthetic enzymes, remains to be investigated.

380 A second co-IP screen was performed with the aim to identify interacting proteins
381 which are specifically inducible. Here, constitutively expressed CYP71A13 was used
382 as a bait and UV-challenged leaves were compared with untreated controls (Fig. 4).
383 Only one of the co-purified proteins was significantly enriched: CYP71B15. In
384 conclusion, CYP71A13-CYP71B15 were robustly identified as a core protein complex
385 and this interaction was confirmed by targeted co-IP and FRET-FLIM (Fig. 5, Fig. 7).

386 The formation of biosynthetic complexes is typically a transient and reversible
387 process (Perkins et al., 2010). For targeted co-IP the bait and interacting proteins
388 were transiently overexpressed, enabling also interactions with proteins of low
389 abundance *in planta*. Here also a CYP71A13-ATR1 interaction was observed.
390 Furthermore, interaction of CYP71A12-CYP79B2 and CYP71A13-CYP79B2 was
391 revealed by FRET-FLIM analysis as this method is most suitable for detecting
392 transient interaction of proteins. As co-IP experiments with microsomal proteins as
393 baits involve solubilisation with mild detergents, cytosolic components of the complex
394 will not directly be solubilized and therefore depleted relative to membrane bound
395 partners. This is probably the case for GGP1, which was not enriched in the
396 untargeted approaches. Similarly, a soluble GST has been proposed as component
397 of the camalexin biosynthetic machinery, but apparently, no GSTs were significantly
398 enriched in an untargeted co-IP with CYP71B15 as bait. For the detection of
399 interactions between known membrane bound and soluble proteins, FRET-FLIM

400 analysis is powerful, as it is not affected by differences in protein solubility. Here, in

401 addition to the interaction of the camalexin biosynthetic cytochrome P450 enzymes,

402 we observed interaction of CYP71A13 with GSTU4 and GGP1 (Fig. 7).

403 Camalexin biosynthesis involves glutathionylation of IAN. As most Arabidopsis GSTs

404 are capable of catalyzing this reaction *in vitro* in concert with CYP71A13

405 (Supplemental Figure 5), it can be postulated that function of a specific GST in

406 camalexin biosynthesis is rather caused by its ability to interact with the biosynthetic

407 machinery or local substrate concentration than by its substrate specificity. *GSTU4* is

408 transcriptionally coregulated with camalexin and tryptophan biosynthetic genes and

409 the corresponding protein was identified as physical interactor of CYP71A13 (Fig. 5,

410 Fig. 7, Supplemental Table 1). Therefore, it was a prime candidate for being a key

411 GST in camalexin biosynthesis. In contrast to this assumption, after infection with *B.*

412 *cinerea*, *gstu4* knockout line had elevated concentrations of camalexin, whereas in

413 overexpression plants, camalexin levels where reduced with respect to wild type

414 leaves. This observation is opposite to the expectations for a camalexin biosynthetic

415 gene. The mechanism by which GSTU4 negatively interferes with camalexin

416 biosynthesis remains unclear. One possibility is that a subcellular transport process is

417 involved, as some GSTs such as GSTF12 (TRANSPARENT TESTA 19), act as

418 transporters between cellular compartments rather than as glutathione transferases

419 (Kitamura et al., 2004; Sun et al., 2012). In this case, an intermediate of the

420 biosynthesis could be exported from the metabolon and metabolized. Alternatively,

421 GSTU4 could have a regulatory function. The human GST Pi acts as inhibitor of Jun

422 N-terminal kinase (JNK). In response to UV irradiation or H_2O_2 treatment GSTp

423 oligomerizes and dissociates from the GSTp–JNK complex (Adler et al., 1999).

424 Whether such GST-dependent activation mechanism in response to stress is relevant

425 also in *Arabidopsis* remains to be investigated. Also, it is unclear whether the

426 interaction between P450/GSTU4 interaction is specific for the camalexin

427 biosynthetic machinery or might play a more general role.

428 In conclusion, CYP79B2, CYP71A12/A13, CYP71B15, and ATR1 form a metabolic

429 complex (Fig. 10). FRET-FLIM data indicated, that, in addition, GGP1 can be

430 recruited to this complex. Based on the data of our untargeted co-IP screens ATR1

431 and CYP79B2 are likely to be less tightly associated with the core camalexin

432 biosynthetic complex. This is in accordance with their different biological functions.

433   ATR1 is required for many different biosynthetic processes in *Arabidopsis*. CYP79B2
434   is also involved in the biosynthesis of indole glucosinolates (Hull et al., 2000;
435   Mikkelsen et al., 2000), the biosynthesis of auxin under specific conditions (Brumos
436   et al., 2014; Tivendale et al., 2014), and the remodeling of root architecture
437   (Julkowska et al., 2017). A possible interaction of CYP79B2 with CYP83B1, which is
438   involved in indole glucosinolate biosynthesis and competes with CYP71A12/A13 for
439   IAOx, was not detected in co-IP and split-ubiquitin-based yeast 2-hybrid screens
440   (Nintemann et al., 2017), potentially indicating a rather weak or temporary protein-
441   protein binding. CYP79B2, a key branch-point enzyme being recruited for different
442   processes is possibly modifying the activities of downstream enzymes. In yeast
443   microsomes expressing CYP71A13 in addition to CYP79B2, the apparent binding
444   constant for the substrate tryptophan was significantly reduced, indicating allosteric
445   interaction and potentially substrate channeling. A similar effect was observed for the
446   entry enzymes of flavonoid biosynthesis (Crosby et al., 2011). For other P450
447   enzymes of the pathway such an effect was not observed. However, they may
448   require Arabidopsis components not present in the heterologous system. Substrate
449   turnover numbers were not determined, as it is typically not possible to purify active
450   membrane bound P450s to homogeneity (Cobbett et al., 1998). Therefore, the
451   amount of mutual activation of catalytic activities might be underestimated and we
452   hypothesize that the camalexin biosynthetic enzymes cooperatively interact to allow
453   high flux to the end product.

454

455   **Material and Methods**

456   Plant growth conditions and stress treatment

457   After stratification for 2 days, *A. thaliana* and *N. benthamiana* plants were grown in a
458   growth chamber under long-day conditions (160 µmol m^{-2} s^{-1}, 16 h light, 8 h dark) at
459   21°C and 50% relative humidity. For induction of phytoalexin biosynthesis *A. thaliana*
460   6-weeks-old rosette leaves were either sprayed with 5 mM $AgNO_3$ or treated with UV-
461   C light for 2 h (Desaga UVVIS; λ= 254 nm, 8 W, distance: 20 cm) or infected with *B.*
462   *cinerea* spores (strain B05.10, 2 × 10^5 spores per ml). Camalexin was extracted after
463   24 h (UV-C and $AgNO_3$ treatment) or 48 h (*B. cinerea* infection).

464

465   Constructs for the expression of fusion proteins

14

466   For generation of CYP71B15-GFP under control of the endogenous promoter, the
467   CYP71B15 promoter (Schuhegger et al., 2006; Chapman et al., 2016) was cloned
468   into pBSK, and the CYP71B15 (At3g26830) CDS was introduced into this plasmid via
469   NcoI/SmaI. The total insert was cut out by EcoRI/SmaI and introduced into pEZS-NL
470   (Carnegie Institution). The promoter-CDS-GFP sequence was cut out with EcoRI
471   /XbaI and introduced into the EcoRI /XbaI pGPTV-BarB vector fragment (Becker et
472   al., 1992).
473   Constructs for YFP- , GFP-, RFP-, and FLAG-tagged proteins were created via the
474   Gateway cloning system (Invitrogen™, Karimi et al. (2005), Katzen (2007)). Genes
475   were amplified from *A. thaliana* cDNA with the listed primers (see below) and cloned
476   into pDONR223. Plasmids were confirmed by sequencing. Based on this LR reaction
477   was performed and constructs were transferred to the destination vectors which
478   contains the 35S promoter and a tag (YFP: pEarlyGate101, GFP: pB7FWG2, RFP:
479   pB7RWG2, FLAG: pEarlyGate202).

480

481   For cloning the following primers were used:

Gene	Primer (5´→3´)
CYP71B15 (At3g26830)	GGGGACAAGTTTGTACAAAAAAGCAGGCTCTTATACTGTGGCTATATATG
	GGGGACCACTTTGTACAAGAAAGCTGGGTTTCCTTGCCCTGTTCTTGTG
CYP71A13 (At2g30770)	GGGGACAAGTTTGTACAAAAAAGCAGGCTTCATGAGCAATATTCAAGAAATGGA
	GGGGACCACTTTGTACAAGAAAGCTGGGTCTTCCACAACCGAAGATGGAAATG
CYP71A12 (At2g30750)	GGGGACAAGTTTGTACAAAAAAGCAGGCTTCATGAGCAATATTCAAGAAATGGA
	GGGGACCACTTTGTACAAGAAAGCTGGGTCTTGAATAACGGAAGATGGAAATGC
CYP79B2 (At4g39950)	GGGGACAAGTTTGTACAAAAAAGCAGGCTTCATGAACACTTTTAC

	GGGGACCACTTTGTACAAGAAAGCTGGGTCCCATCACTTCAC CGT
ATR1 (At4g24520)	GGGGACAAGTTTGTACAAAAAGCAGGCTTCATGACTTCTGCT TTGTATGCTTCC
	GGGGACCACTTTGTACAAGAAAGCTGGGTCCTATCACCAGAC ATCTCTGAGGTATC
GSTU2 (At2g29480)	GGGGACAAGTTTGTACAAAAAGCAGGCTTCATGGCGAAGAA AGAAGAGAGT
	GGGGACCACTTTGTACAAGAAAGCTGGGTCTTCGAACGTAGA CTTAGCTCT
GSTU4 (At2g29460)	GGGGACAAGTTTGTACAAAAAGCAGGCTTCATGGCGGAGAA AGAAGAGGATGTG
	GGGGACCACTTTGTACAAGAAAGCTGGGTCTTCGGCTGATTT GATTCTTTCTACC

482

483

Generation of transgenic *Arabidopsis* lines

A. thaliana accession Columbia was transformed with *Agrobacteria* harboring the *CYP71B15*$_{pro}$*:CYP71B15*-GFP expression construct via floral dip (Clough and Bent, 1998). Phosphinothricin (PPT)-resistant primary transformants were confirmed by PCR and qualitatively screened for GFP fluorescence in response to AgNO$_3$ spraying. A high-expression line was crossed to the *cyp71b15/pad3* T-DNA insertion line SALK_026585 (Xu et al., 2008; Lemarié et al., 2015) and from the F2 generation homozygous *pad3* / *CYP71B15*$_{pro}$*:CYP71B15*-GFP plants were selected which carried the construct and, at least partially, complemented the camalexin-deficient *pad3* phenotype (Supplemental Figure 1B). The progeny of one individual was used for proteomics analysis. For constitutive expression of CYP71A13-YFP, a corresponding pEarleyGate101 construct was used. Replicates represent independent microsome preparations from independent plants.

497

Analysis of *CYP71B15*-GFP localization in response to pathogens

16

499   The *B. cinerea* strain B05.10 was cultivated on potato dextrose agar (PDA) under
500   UV-light (12 h darkness, 12 h light) at RT. Preparation of *B. cinerea* spore
501   suspension and inoculation procedure followed instructions in Gronover et al. (2001)
502   using 10 µl droplets of a suspension of 8 x 10^5 conidia per ml on fully developed
503   Arabidopsis leaves. *A. brassicicola* was grown on synthetic nutrient-poor agar (SNA,
504   (Nirenberg, 1981) under UV-light. Fully developed Arabidopsis leaves were
505   inoculated with 10 µl droplets of a suspension of $5x10^4$ spores per ml H_2O / 0.02%
506   (v/v) Tween20. Plants infected with *B. cinerea* or *A. brassicicola* were cultivated
507   under normal growth conditions in a closed box in order to retain high humidity.
508   For infection with *E. cruciferarum*, Arabidopsis plants were placed under an
509   inoculation box covered with a polyamide net (0.2 mm^2) and inoculated at a density
510   of 3-5 conidia per mm^2 by brushing conidia off of powdery mildew infected plants.
511   *E. cruciferarum* membranes were stained with 20 µM SynaptoRed™ C2 (also known
512   as FM-464, Sigma-Aldrich) for 15 min in the dark. Images were taken with a confocal
513   laser-scanning microscope (Leica SP5). GFP was excited with a 488 nm laser line
514   and detected between 500 and 530 nm, SynaptoRed™ was excited at 561 nm and
515   detected between 600 and 645 nm.

516

517   Transient expression in *Nicotiana benthamiana*

518   For transient protein expression in *Nicotiana benthamiana,* expression plasmids were
519   transformed into *Agrobacterium tumefaciens GV3101(MP90).* Correct transformants
520   were confirmed by PCR specific for the transgene. 25 ml overnight cultures were
521   centrifuged and resuspended in 10 mM MES, 10 mM $MgCl_2$, 150 µM acetosyringone,
522   pH=5.6 at an OD_{600} of 0.5-0.6. The cells are then incubated in a shaker for 2 h (RT)
523   and the cultures of *Agrobacterium* expressing the possibly interacting proteins and
524   the supporting strain p19 were mixed in the ratio 1:1:1 (Sparkes et al., 2006). For
525   each sample 4-6 leaves of *N. benthamiana* were infiltrated on the abaxial side of the
526   leaves with a 1 ml syringe. After infiltration, before harvesting the infiltrated leaves,
527   the plants were incubated for 3 d in a growth chamber under long-day conditions
528   (160 µmol m^{-2} s^{-1}, 16 h light, 8 h dark) at 21°C.

529

530   Plant microsome generation and co-immunoprecipitation

531 Infiltrated leaves were harvested and ground with a mix of sea sand and Polyklar®
532 AT (Serva) (ratio 1:1) and 5 ml of ice-cold buffer 1 (100 mM ascorbic acid, 50 mM
533 Na_2SO_4, 250 mM Tricin, 2 mM EDTA, DTE 2 mM, 5 g/L BSA, pH 8,2). 20 ml of buffer
534 1 was added and the homogenate was centrifuged (20,000xg, 4°C, 10 min). The
535 supernatant was filtrated via a gauze bandage and centrifuged again. Microsomes
536 were pelletized by centrifugation (60000xg, 4°C, 2 h) and in 1.5 ml buffer 2 (50 mM
537 NaCl, 100 mM Tricin, 250 mM sucrose, 2 mM EDTA, 2 mM DTE, pH 8,2)
538 resuspended.

539 For solubilisation, 500 µl microsomes were mixed with Triton X-100 to a final
540 concentration of 0.5%. The samples are incubated at 4°C for 1 h under constant
541 shaking and centrifuged (20000xg, 1.5 h, 4°C). The supernatant was transferred to a
542 new Eppendorf tube and protein concentration determined photometrically (BIO-RAD
543 Protein Assay).

544 For untargeted co-IP, GFP-Trap® A beads (Chromotek, Munich, Germany; Rothbauer
545 et al. (2008)) were equilibrated with co-IP buffer (10 mM Tris; 150 mM NaCl; 0.5 mM
546 EDTA) and mixed with 1 volume microsomes solubilized in 1% Triton X-100 (100 µl
547 beads in a total volume of 4 ml for bait expressed under endogenous promoter, 50 µl
548 beads / 2 ml for bait expressed under the 35S promoter). After incubation for 1 h at
549 4°C under constant shaking, beads were centrifuged (2700xg, 4°C, 2 min) and
550 washed three times with co-IP buffer. The supernatant was replaced by 30 µl
551 NuPAGE® LDS Sample Buffer (4x, Invitrogen GmbH, Karlsruhe, Germany) together
552 with 30 µl 100 mM DTT and incubated at 70°C for 15 min. Targeted co-IP was
553 performed with 10 µl GFP-Trap® A beads each, in a total volume of 500 µl. The
554 samples were analyzed via western blot using anti-FLAG (Sigma, F1804) and anti-
555 GFP (Invitrogen, A-11122) antibody followed by staining with goat anti-mouse HRP
556 (Bio-Rad, 172-1011) or goat anti-rabbit HRP (Life Technologies, 65-6120)
557 respectively (dilution of all antibodies 1:3000). Replicates represent independent
558 microsome preparations from independent plants.

559

560 Protein identification by liquid chromatography and tandem mass spectrometry (LC-
561 MS/MS)

562 *In-gel digestion*

563   Protein samples were reduced by 10 mM dithiothreitol, and alkylated by 55 mM

564   iodoacetamide (CYP71B15 dataset) or 55 mM chloroacetamide (CYP71A13 dataset).

565   Proteins were run into a 4–12% NuPAGE gel for about 1 cm to concentrate the

566   sample prior to in-gel tryptic digestion. In-gel trypsin digestion was performed

567   according to standard procedures (Shevchenko et al., 2006).

568   *LC-MS/MS analysis of CYP71B15 experiments*

569   Peptides generated by in-gel trypsin digestion were analyzed via LC-MS/MS on a

570   nanoLC-Ultra 1D+ (Eksigent, Dublin, CA) coupled to an LTQ-Orbitrap Elite mass

571   spectrometer (ThermoFisher Scientific). Peptides were delivered to a trap column

572   (Reprosil-Pur C18 ODS3 5 µm resin, Dr. Maisch, Ammerbuch, Germany, 20 mm × 75

573   µm, self-packed) at a flow rate of 5 µl/min in 100% solvent A_0 (0.1% formic acid in

574   HPLC grade water). Peptides were then transferred to an analytical column

575   (Reprosil-Gold C18 120, 3 µm, Dr. Maisch, Ammerbuch, Germany, 400 mm × 75 µm,

576   self-packed) and separated using a 110 min gradient from 4% to 32% solvent B

577   (0.1% formic acid and 5% DMSO in acetonitrile) in A (0.1% formic acid and 5%

578   DMSO in HPLC grade water) at a flow rate of 300 nl/min. The mass spectrometer

579   was operated in data dependent mode, automatically switching between MS and

580   MS2 spectra. Up to 15 peptide precursors were subjected to fragmentation by higher

581   energy collision-induced dissociation (HCD) and analyzed in the Orbitrap. Dynamic

582   exclusion was set to 20 s.

583   *LC-MS/MS analysis of CYP71A13 experiments*

584   Peptides generated by in-gel trypsin digestion were analyzed via LC-MS/MS on a

585   nanoLC-Ultra 1D+ (Eksigent, Dublin, CA) coupled to a Q Exactive HF mass

586   spectrometer (ThermoFisher Scientific). Peptides were delivered to a trap column

587   (75 µm x 2 cm, packed in house with Reprosil-Pur C18 ODS3 5 µm resin, Dr.

588   Maisch) for 10 min at a flow rate of 5 µl/min in 100% solvent A_0 (0.1% formic acid in

589   HPLC grade water). Peptides were then separated on an analytical column (75 µm x

590   40 cm, packed in-house with Reprosil-Gold C18 120, 3 µm resin, Dr. Maisch) using a

591   120 min gradient ranging from 4-32% solvent B (0.1% formic acid and 5% DMSO in

592   acetonitrile) in A (0.1% formic acid and 5% DMSO in HPLC grade water) at a flow

593   rate of 300 nl/min. The mass spectrometer was operated in data dependent mode,

594   automatically switching between MS and MS2 spectra. Up to 20 peptide precursors

595   were subjected to fragmentation by higher energy collision-induced dissociation

596   (HCD) and analyzed in the Orbitrap. Dynamic exclusion was set to 20 s.

Peptide and protein identification and quantification

598   Label free quantification was performed using MaxQuant (version 1.6.1.0) (Cox and

599   Mann, 2008) by searching MS data against an *Arabidopsis thaliana* reference

600   database derived from UniProt (version 09.07.2016, 31424 entries) using the

601   embedded search engine Andromeda (Cox et al., 2011). Carbamidomethylated

602   cysteine was used as fixed modification; variable modifications included oxidation of

603   methionine and N-terminal protein acetylation. Trypsin/P was specified as proteolytic

604   enzyme with up to two allowed missed cleavage sites. Precursor tolerance was set to

605   10 ppm and fragment ion tolerance was set to 20 ppm. Label-free quantification (Cox

606   et al., 2014), match-between-runs and intensity-based absolute quantification options

607   were enabled and results were filtered for a minimal length of seven amino acids, 1%

608   peptide and protein FDR as well as common contaminants and reverse

609   identifications.

Data analysis and visualization

611   MaxQuant results were imported into the MaxQuant associated software suite

612   Perseus (v.1.5.8.5) (Tyanova and Cox, 2018). Label-free quantification intensities

613   (LFQ) were filtered for at least 3 valid values for at least one experimental group and

614   at least 3 peptides for identification per protein. Missing values were imputed from

615   normal distribution (width 0.2, downshift 2.0). A two-sided unpaired student's t-test

616   was performed to assess statistical significance. Protein p-values were corrected for

617   multiple testing using a permutation based 1% FDR cut-off (1000 permutations).

618   Standard functions in the SAM R-package were used to adjust s0 for each dataset

619   (Tusher et al., 2001). For the CYP71B15 scatter plots proteins were filtered for at

620   least 2 valid values for at least one experimental group and at least 3 peptides for

621   identification per protein. Means were calculated and missing values were imputed by

622   a constant (constant: 0).

Data deposition

624   Mass spectrometry data have been deposited to the ProteomeXchange Consortium

625   (http://proteomecentral.proteomexchange.org) via the PRIDE partner repository

626   (Vizcaíno et al., 2012) with the dataset identifier PXD008812 (reviewer account:

627   username: reviewer70359@ebi.ac.uk, password: MRXOTnDO).

628

<u>Yeast transformation, protein expression, yeast microsomes, enzyme analysis and yeast feeding experiments</u>

The *Saccharomyces cerevisiae* strain BY4741 (Brachmann et al., 1998), auxotroph for His, Leu, Met and Ura, was used for coexpression of ATR1 (on plasmid pGREG505), CYP79B2 (on plasmid pYeDP60) and CYP71A13 (on plasmid pSH62) or the corresponding vector control. Transformations were performed according to Gietz et al. (1992). Yeasts were cultivated and microsomes were prepared essentially as described by (Schuhegger et al., 2006) , with the modification that instead of SGIW medium the selection medium SD was used (Amberg et al., 2005). Microsomes were resuspended in TEG buffer (50 mM Tris pH 7.5, 1 mM EDTA, 20% glycerol, 2 mM DTE) and incubated with 0.5 mM NADPH and 5-200 µM of tryptophan for 45 to 90 min. To stop the reaction 2 Vol. of 100% methanol were added and the reaction mix was centrifuged twice to remove macroscopic contaminants. The conversion of tryptophan to indole-3-acetaldoxime was monitored by reverse-phase HPLC (Lichrosphere 100 RP-18, 250 x 3 mm, 5 µM, Merck; flow rate of 0.6 mL min-1; solvents, 0.3% (v/v) formic acid in water (A) and acetonitrile (B); gradient: 0 to 2 min, isocratic, 25% B; 2 to 10.5 min, linear from 25% to 45% B; 10.5 to 13 min, linear from 45% to 100% B; 13 to 15 min, isocratic, 100% B) and quantified based on a calibration curve of the authentic standard (Glawischnig et al., 2004). Determination of K_m values was performed via GraphPad PrismGraph (Michaelis-Menten analysis).

For feeding experiments yeasts carrying ATR1 (on plasmid pGREG505), CYP71A13 (on plasmid pYeDP60) and one out of 54 GSTs (on plasmid pSH62) were grown in SD medium with appropriate supplements (-His, -Leu, -Met, -Ura) until OD_{600} = 0.6 was reached. Protein expression was induced by addition of galactose for 16 h. Feeding was performed with 0.1 mM IAN and 0.2 mM GSH for 24 h. Subsequently yeast cells were harvested, washed in ddH_2O, and 350 µl methanol:formic acid; 99.8%:0.2% (v/v) was added. After vortexing and incubation at room temperature for 15 min under constant shaking cell debris were removed and GS-IAN formation analyzed via HPLC (Lichrosphere 100 RP-18, 250 x 3 mm, 5 µM, Merck; flow rate of 0.6 mL min-1; solvents, 0.3% (v/v) formic acid in water (A) and acetonitrile (B); gradient: 0 to 2 min, isocratic, 25% B; 2 to 19 min, linear from 25% to 50% B; 19 to 24 min, linear from 50% to 100% B; 24 to 26 min, isocratic, 100% B), calibrating with

661　the authentic standard.

662

663　<u>Confocal microscopy and FRET-FLIM analysis</u>

664　For co-localization experiments leaf epidermal samples were imaged using a Zeiss

665　PlanApo ×100/1.46 NA oil immersion objective on a Zeiss LSM880 confocal

666　equipped with an Airyscan detector. 512 × 512 images were collected in 8-bit with 2-

667　line averaging at an (x,y) pixel spacing of 20–80 nm with excitation at 488 nm (GFP)

668　and 561 nm (RFP), and emission at 495–550 nm and 570–615 nm, respectively.

669　Data was produced from at least three independent biological replicates, defined as

670　separate plants independently infiltrated from glycerol stocks. At least twenty cells

671　per combination were imaged in a randomized manner.

672　FRET-FLIM analysis was performed according to Kriechbaumer et al. (2015). In brief:

673　Epidermal samples of infiltrated leaves were excised and multiphoton FRET-FLIM

674　data capture was performed by a two-photon microscope built around a Nikon

675　TE2000-U inverted microscope with a modified Nikon EC2 confocal scanning system.

676　Laser light at a wavelength of 920 nm was produced by a mode-locked titanium

677　sapphire laser (Mira; Coherent Lasers), with 200-fs pulses at 76 MHz, pumped by a

678　solid-state continuous wave 532-nm laser (Verdi V18; Coherent Laser). The laser

679　beam was focused to a diffraction limited spot using a water-immersion objective

680　(Nikon VC; 360, numerical aperture of 1.2). Fluorescence emission was collected

681　bypassing the scanning system and passed through a BG39 (Comar) filter to block

682　the near-infrared laser light. Line, frame, and pixel clock signals were generated and

683　synchronized with an external detector in the form of a fast microchannel plate

684　photomultiplier tube (Hamamatsu R3809U). Raw FRET-FLIM data was generated by

685　linking these via a time-correlated single-photon counting PC module SPC830

686　(Becker and Hickl). Prior to FLIM data collection, the GFP and mRFP expression

687　levels in the plant samples within the region of interest were confirmed using a Nikon

688　EC2 confocal microscope with excitation at 488 and 543 nm, respectively. A 633-nm

689　interference filter is used to significantly minimize the contaminating effect of

690　chlorophyll autofluorescence emission.

691　Data were analyzed by obtaining excited-state lifetime values first on a pixel by pixel

692　basis, then of a region of interest on the nuclear envelope, and calculations were

693　made using SPCImage analysis software version 5.1. The distribution of lifetime

values within the region of interest was generated and displayed as a curve. Only values with a χ^2 between 0.9 and 1.4 were considered. The median lifetime, minimum and maximum values for one-quarter of the median lifetime values from the curve were taken to generate the range of lifetimes per sample. Data from a minimum of three independent biological replicas and at least five nuclei per replica and per protein-protein combination were analyzed, and the average of the ranges was taken. Biological replicas are defined as separate plants independently infiltrated and analyzed.

Camalexin extraction

Camalexin extraction was performed according to (Müller et al., 2015). In brief, leaves were weighed and 400 µl of methanol:water (80:20, v/v) was added. After incubation for 1 h at 65°C under constant shaking, extracts were cleaned twice via centrifugation and analyses by reverse-phase HPLC (MultoHigh 100 RP18, 5-mm particle size; Göhler Analytik).

Author contributions

S.M. designed and conducted the majority of experiments; S.H. performed proteomics analysis under the guidance of B.K.; V.K. performed FRET-FLIM and colocalization studies; B.S. and E.Gl. performed P450 expression in yeast; C.K. and M.C. generated lines for untargeted co-IP; M.C. and E.Gl. performed untargeted co-IP; N.K., under the guidance of E.Gr., generated yeast strains expressing GSTs; R. E. performed confocal microscopic analysis of pathogen infected material under the guidance of R. H.. E. Gl. designed and supervised the overall project; E.Gl. and S.M. wrote the article with contributions of all authors.

Figure Legends

Fig.1: Biosynthetic pathway of camalexin and related metabolites

Fig.2: CYP71B15-GFP accumulates in cells surrounding fungal infection sites

Fig. 3: Proteins co-purified with CYP71B15-GFP from leaves infected with *B. cinerea*

Fig. 4: Proteins co-purified from leaves overexpressing CYP71A13 with or without UV irradiation

Fig. 5: Co-IP analysis of the physical association of camalexin-specific enzymes

Fig. 6: Co-localization of camalexin-specific enzymes in *N. benthamiana* leaves

Fig. 7: Tight physical interaction of camalexin-biosynthesis enzymes supported by Förster Resonance Energy Transfer studies combined with Fluorescence Life Time Microscopy (FRET-FLIM)

Fig. 8: Higher apparent substrate affinity of CYP79B2 by presence of CYP71A13

Fig. 9: Camalexin formation in response to *B. cinerea* infection in *gstu4* knockout and overexpression plants

Fig. 10: Model of a camalexin-biosynthetic metabolon

References

Adler, V., Yin, Z., Fuchs, S.Y., Benezra, M., Rosario, L., Tew, K.D., Pincus, M.R., Sardana, M., Henderson, C.J., and Wolf, C.R. (1999). Regulation of JNK signaling by GSTp. The EMBO journal **18,** 1321-1334.

Amberg, D.C., Burke, D.J., and Strathern, J.N. (2005). Methods in Yeast Genetics: A Cold Spring Harbor Laboratory Course Manual, 2005 Edition (Cold Spring).

Bak, S., Tax, F.E., Feldmann, K.A., Galbraith, D.W., and Feyereisen, R. (2001). CYP83B1, a cytochrome P450 at the metabolic branch point in auxin and indole glucosinolate biosynthesis in Arabidopsis. The Plant Cell **13,** 101-111.

Bak, S., Beisson, F., Bishop, G., Hamberger, B., Höfer, R., Paquette, S., and Werck-Reichhart, D. (2011). Cytochromes P450. The Arabidopsis Book, e0144.

Bassard, J.E., Richert, L., Geerinck, J., Renault, H., Duval, F., Ullmann, P., Schmitt, M., Meyer, E., Mutterer, J., Boerjan, W., De Jaeger, G., Mely, Y., Goossens, A., and Werck-Reichhart, D. (2012). Protein-protein and protein-membrane associations in the lignin pathway. Plant Cell **24,** 4465-4482.

Becker, D., Kemper, E., Schell, J., and Masterson, R. (1992). New plant binary vectors with selectable markers located proximal to the left T-DNA border. Plant Molecular Biology **20,** 1195-1197.

Becker, W. (2012). Fluorescence lifetime imaging–techniques and applications. Journal of Microscopy **247,** 119-136.

Bednarek, P., Schneider, B., Svatoš, A., Oldham, N.J., and Hahlbrock, K. (2005). Structural complexity, differential response to infection, and tissue specificity of indolic and phenylpropanoid secondary metabolism in Arabidopsis roots. Plant Physiology **138,** 1058-1070.

Böttcher, C., Westphal, L., Schmotz, C., Prade, E., Scheel, D., and Glawischnig, E. (2009). The multifunctional enzyme CYP71B15 (PHYTOALEXIN DEFICIENT3) converts cysteine-indole-3-acetonitrile to camalexin in the indole-3-acetonitrile metabolic network of Arabidopsis thaliana. Plant Cell **21,** 1830-1845.

Böttcher, C., Chapman, A., Fellermeier, F., Choudhary, M., Scheel, D., and Glawischnig, E. (2014). The Biosynthetic Pathway of Indole-3-Carbaldehyde and Indole-3-Carboxylic Acid Derivatives in Arabidopsis. Plant Physiol **165,** 841-853.

Brachmann, C.B., Davies, A., Cost, G.J., Caputo, E., Li, J., Hieter, P., and Boeke, J.D. (1998). Designer deletion strains derived from Saccharomyces cerevisiae S288C: a useful set of strains and plasmids for PCR-mediated gene disruption and other applications. Yeast **14,** 115-132.

Brumos, J., Alonso, J.M., and Stepanova, A.N. (2014). Genetic aspects of auxin biosynthesis and its regulation. Physiologia Plantarum **151,** 3-12.

Chapman, A., Lindermayr, C., and Glawischnig, E. (2016). Expression of antimicrobial peptides under control of a camalexin-biosynthetic promoter confers enhanced resistance against Pseudomonas syringae. Phytochemistry **122,** 76-80.

Clough, S.J., and Bent, A.F. (1998). Floral dip: a simplified method for Agrobacterium-mediated transformation of Arabidopsis thaliana. Plant Journal **16,** 735-743.

Cobbett, C.S., May, M.J., Howden, R., and Rolls, B. (1998). The glutathione-deficient, cadmium-sensitive mutant, cad2-1, of Arabidopsis thaliana is deficient in gamma-glutamylcysteine synthetase. Plant J **16,** 73-78.

Cox, J., and Mann, M. (2008). MaxQuant enables high peptide identification rates, individualized ppb-range mass accuracies and proteome-wide protein quantification. Nature Biotechnology **26,** 1367.

Cox, J., Neuhauser, N., Michalski, A., Scheltema, R.A., Olsen, J.V., and Mann, M. (2011). Andromeda: a peptide search engine integrated into the MaxQuant environment. Journal of Proteome Research **10,** 1794-1805.

Cox, J., Hein, M.Y., Luber, C.A., Paron, I., Nagaraj, N., and Mann, M. (2014). Accurate Proteome-wide Label-free Quantification by Delayed Normalization and Maximal Peptide Ratio Extraction, Termed MaxLFQ. Molecular & Cellular Proteomics **13,** 2513-2526.

Crosby, K.C., Pietraszewska-Bogiel, A., Gadella, T.W., Jr., and Winkel, B.S. (2011). Forster resonance energy transfer demonstrates a flavonoid metabolon in living plant cells that displays competitive interactions between enzymes. FEBS Letters **585,** 2193-2198.

Czerniawski, P., and Bednarek, P. (2018). Glutathione S-Transferases in the Biosynthesis of Sulfur-Containing Secondary Metabolites in Brassicaceae Plants. Front Plant Sci **9,** 1639.

Dastmalchi, M., Bernards, M.A., and Dhaubhadel, S. (2016). Twin anchors of the soybean isoflavonoid metabolon: evidence for tethering of the complex to the endoplasmic reticulum by IFS and C4H. The Plant Journal **85,** 689-706.

816   **Davydov, D.R., Davydova, N.Y., Sineva, E.V., and Halpert, J.R.** (2015). Interactions among cytochromes
817   P450 in microsomal membranes: oligomerization of cytochromes P450 3A4, 3A5, and 2E1 and its
818   functional consequences. Journal of Biological Chemistry **290,** 3850-3864.
819   **Dixon, D.P., Lapthorn, A., and Edwards, R.** (2002). Plant glutathione transferases. Genome Biology **3,**
820   reviews3004. 3001.
821   **Förster, T.** (1948). Zwischenmolekulare Energiewanderung und Fluoreszenz. Annalen der Physik **437,**
822   55-75.
823   **Frerigmann, H., Pislewska-Bednarek, M., Sanchez-Vallet, A., Molina, A., Glawischnig, E., Gigolashvili,**
824   **T., and Bednarek, P.** (2016). Regulation of Pathogen-Triggered Tryptophan Metabolism in Arabidopsis
825   thaliana by MYB Transcription Factors and Indole Glucosinolate Conversion Products. Mol Plant **9,** 682-
826   695.
827   **Fuchs, R., Kopischke, M., Klapprodt, C., Hause, G., Meyer, A.J., Schwarzlander, M., Fricker, M.D., and**
828   **Lipka, V.** (2016). Immobilized Subpopulations of Leaf Epidermal Mitochondria Mediate PENETRATION2-
829   Dependent Pathogen Entry Control in Arabidopsis. The Plant cell **28,** 130-145.
830   **Fujino, N., Tenma, N., Waki, T., Ito, K., Komatsuzaki, Y., Sugiyama, K., Yamazaki, T., Yoshida, S.,**
831   **Hatayama, M., Yamashita, S., Tanaka, Y., Motohashi, R., Denessiouk, K., Takahashi, S., and**
832   **Nakayama, T.** (2018). Physical interactions among flavonoid enzymes in snapdragon and torenia reveal
833   the diversity in the flavonoid metabolon organization of different plant species. Plant J **94,** 372-392.
834   **Gietz, D., St Jean, A., Woods, R.A., and Schiestl, R.H.** (1992). Improved method for high efficiency
835   transformation of intact yeast cells. Nucleic Acids Research **20,** 1425.
836   **Glawischnig, E., Hansen, B.G., Olsen, C.E., and Halkier, B.A.** (2004). Camalexin is synthesized from
837   indole-3-acetaldoxime, a key branching point between primary and secondary metabolism in Arabidopsis.
838   Proceedings of the National Academy of Sciences **101,** 8245-8250.
839   **Glazebrook, J., and Ausubel, F.M.** (1994). Isolation of phytoalexin-deficient mutants of Arabidopsis
840   thaliana and characterization of their interactions with bacterial pathogens. Proceedings of the National
841   Academy of Sciences **91,** 8955-8959.
842   **Gronover, C.S., Kasulke, D., Tudzynski, P., and Tudzynski, B.** (2001). The role of G protein alpha
843   subunits in the infection process of the gray mold fungus Botrytis cinerea. Mol Plant Microbe Interact **14,**
844   1293-1302.
845   **Hansen, C.H., Du, L., Naur, P., Olsen, C.E., Axelsen, K.B., Hick, A.J., Pickett, J.A., and Halkier, B.A.**
846   (2001). CYP83B1 is the oxime-metabolizing enzyme in the glucosinolate pathway in Arabidopsis. Journal
847   of Biological Chemistry **276,** 24790-24796.
848   **Hawes, C., and Kriechbaumer, V.** (2018). The Plant Endoplasmic Reticulum. (Springer).
849   **He, Y., Xu, J., Wang, X., He, X., Wang, Y., Zhou, J., Zhang, S., and Meng, X.** (2019). The Arabidopsis
850   Pleiotropic Drug Resistance Transporters PEN3 and PDR12 Mediate Camalexin Secretion for Resistance to
851   Botrytis cinerea. The Plant cell.
852   **Julkowska, M., Koevoets, I.T., Mol, S., Hoefsloot, H.C., Feron, R., Tester, M., Keurentjes, J.J., Korte, A.,**
853   **Haring, M.A., and de Boer, G.-J.** (2017). Genetic Components of Root Architecture Remodeling in
854   Response to Salt Stress. The Plant Cell**,** tpc. 00680.02016.
855   **Karimi, M., De Meyer, B., and Hilson, P.** (2005). Modular cloning in plant cells. Trends in Plant Science
856   **10,** 103-105.
857   **Katzen, F.** (2007). Gateway® recombinational cloning: a biological operating system. Expert Opinion on
858   Drug Discovery **2,** 571-589.
859   **Kitamura, S., Shikazono, N., and Tanaka, A.** (2004). TRANSPARENT TESTA 19 is involved in the
860   accumulation of both anthocyanins and proanthocyanidins in Arabidopsis. The Plant Journal **37,** 104-114.
861   **Klein, A.P., Anarat-Cappillino, G., and Sattely, E.S.** (2013). Minimum Set of Cytochromes P450 for
862   Reconstituting the Biosynthesis of Camalexin, a Major Arabidopsis Antibiotic. Angewandte Chemie
863   International Edition **52,** 13625-13628.
864   **Knudsen, C., Gallage, N.J., Hansen, C.C., Moller, B.L., and Laursen, T.** (2018). Dynamic metabolic
865   solutions to the sessile life style of plants. Nat Prod Rep **35,** 1140-1155.
866   **Kowalski, N.A.** (2016). Charakterisierung der Glutathiontransferasen aus Arabidopsis thaliana. In
867   Fakultät Wissenschaftszentrum Weihenstephan (Freising: TU-München), pp. 216.
868   **Krajewski, M.P., Kanawati, B., Fekete, A., Kowalski, N., Schmitt-Kopplin, P., and Grill, E.** (2013).
869   Analysis of Arabidopsis glutathione-transferases in yeast. Phytochemistry **91,** 198-207.
870   **Kriechbaumer, V., Botchway, S.W., Slade, S.E., Knox, K., Frigerio, L., Oparka, K., and Hawes, C.** (2015).
871   Reticulomics: Protein-Protein Interaction Studies with Two Plasmodesmata-Localized Reticulon Family
872   Proteins Identify Binding Partners Enriched at Plasmodesmata, Endoplasmic Reticulum, and the Plasma
873   Membrane. Plant Physiology **169,** 1933-1945.

874   **Kutz, A., Müller, A., Hennig, P., Kaiser, W.M., Piotrowski, M., and Weiler, E.W.** (2002). A role for
875   nitrilase 3 in the regulation of root morphology in sulphur-starving Arabidopsis thaliana. The Plant
876   Journal **30,** 95-106.
877   **Lallemand, B., Erhardt, M., Heitz, T., and Legrand, M.** (2013). Sporopollenin biosynthetic enzymes
878   interact and constitute a metabolon localized to the endoplasmic reticulum of tapetum cells. Plant
879   physiology **162,** 616-625.
880   **Laursen, T., Borch, J., Knudsen, C., Bavishi, K., Torta, F., Martens, H.J., Silvestro, D., Hatzakis, N.S.,**
881   **Wenk, M.R., and Dafforn, T.R.** (2016). Characterization of a dynamic metabolon producing the defense
882   compound dhurrin in sorghum. Science **354,** 890-893.
883   **Lemarié, S., Robert-Seilaniantz, A., Lariagon, C., Lemoine, J., Marnet, N., Levrel, A., Jubault, M.,**
884   **Manzanares-Dauleux, M.J., and Gravot, A.** (2015). Camalexin contributes to the partial resistance of
885   Arabidopsis thaliana to the biotrophic soilborne protist Plasmodiophora brassicae. Frontiers in plant
886   science **6**.
887   **Mikkelsen, M.D., Hansen, C.H., Wittstock, U., and Halkier, B.A.** (2000). Cytochrome P450 CYP79B2
888   from Arabidopsis catalyzes the conversion of tryptophan to indole-3-acetaldoxime, a precursor of indole
889   glucosinolates and indole-3-acetic acid. Journal of Biological Chemistry **275,** 33712-33717.
890   **Müller, T.M., Böttcher, C., and Glawischnig, E.** (2019). Dissection of the network of indolic defence
891   compounds in Arabidopsis thaliana by multiple mutant analysis. Phytochemistry **161,** 11-20.
892   **Müller, T.M., Böttcher, C., Morbitzer, R., Götz, C.C., Lehmann, J., Lahaye, T., and Glawischnig, E.**
893   (2015). Transcription activator-like effector nuclease-mediated generation and metabolic analysis of
894   camalexin-deficient cyp71a12 cyp71a13 double knockout lines. Plant Physiology **168,** 849-858.
895   **Nafisi, M., Goregaoker, S., Botanga, C.J., Glawischnig, E., Olsen, C.E., Halkier, B.A., and Glazebrook, J.**
896   (2007). Arabidopsis cytochrome P450 monooxygenase 71A13 catalyzes the conversion of indole-3-
897   acetaldoxime in camalexin synthesis. The Plant cell **19,** 2039-2052.
898   **Nintemann, S.J., Vik, D., Svozil, J., Bak, M., Baerenfaller, K., Burow, M., and Halkier, B.A.** (2017).
899   Unravelling protein-protein interaction networks linked to aliphatic and indole glucosinolate biosynthetic
900   pathways in Arabidopsis. Frontiers in Plant Science **8**.
901   **Nirenberg, H.I.** (1981). A simplified method for identifying Fusarium spp. occuring on wheat. Canadian
902   Journal of Botany **59,** 1599-1609.
903   **Parisy, V., Poinssot, B., Owsianowski, L., Buchala, A., Glazebrook, J., and Mauch, F.** (2007).
904   Identification of PAD2 as a γ-glutamylcysteine synthetase highlights the importance of glutathione in
905   disease resistance of Arabidopsis. The Plant Journal **49,** 159-172.
906   **Perkins, J.R., Diboun, I., Dessailly, B.H., Lees, J.G., and Orengo, C.** (2010). Transient protein-protein
907   interactions: structural, functional, and network properties. Structure **18,** 1233-1243.
908   **Rajniak, J., Barco, B., Clay, N.K., and Sattely, E.S.** (2015). A new cyanogenic metabolite in Arabidopsis
909   required for inducible pathogen defence. Nature **525,** 376-379.
910   **Rauhut, T.** (2009). Die Regulation der Camalexinbiosynthese in Arabidopsis thaliana. In Lehrstuhl für
911   Genetik (Freising: TU-München).
912   **Rauhut, T., and Glawischnig, E.** (2009). Evolution of camalexin and structurally related indolic
913   compounds. Phytochemistry **70,** 1638-1644.
914   **Reed, J.R., and Backes, W.L.** (2012). Formation of P450· P450 complexes and their effect on P450
915   function. Pharmacology & Therapeutics **133,** 299-310.
916   **Rothbauer, U., Zolghadr, K., Muyldermans, S., Schepers, A., Cardoso, M.C., and Leonhardt, H.** (2008).
917   A versatile nanotrap for biochemical and functional studies with fluorescent fusion proteins. Molecular &
918   Cellular Proteomics **7,** 282-289.
919   **Schlaeppi, K., Abou-Mansour, E., Buchala, A., and Mauch, F.** (2010). Disease resistance of Arabidopsis
920   to Phytophthora brassicae is established by the sequential action of indole glucosinolates and camalexin.
921   The Plant Journal **62,** 840-851.
922   **Schoberer, J., and Botchway, S.W.** (2014). Investigating protein-protein interactions in the plant
923   endomembrane system using multiphoton-induced FRET-FLIM. Methods in Molecular Biology **1209,** 81-
924   95.
925   **Schuhegger, R., Nafisi, M., Mansourova, M., Petersen, B.L., Olsen, C.E., Svatos, A., Halkier, B.A., and**
926   **Glawischnig, E.** (2006). CYP71B15 (PAD3) catalyzes the final step in camalexin biosynthesis. Plant
927   Physiology **141,** 1248-1254.
928   **Shevchenko, A., Tomas, H., Havli, J., Olsen, J.V., and Mann, M.** (2006). In-gel digestion for mass
929   spectrometric characterization of proteins and proteomes. Nature Protocols **1,** 2856.
930   **Sønderby, I.E., Geu-Flores, F., and Halkier, B.A.** (2010). Biosynthesis of glucosinolates–gene discovery
931   and beyond. Trends in plant science **15,** 283-290.

932 **Sparkes, I.A., Runions, J., Kearns, A., and Hawes, C.** (2006). Rapid, transient expression of fluorescent
933 fusion proteins in tobacco plants and generation of stably transformed plants. Nature Protocols **1,** 2019-
934 2025.
935 **Su, T.B., Xu, J.A., Li, Y.A., Lei, L., Zhao, L., Yang, H.L., Feng, J.D., Liu, G.Q., and Ren, D.T.** (2011).
936 Glutathione-Indole-3-Acetonitrile Is Required for Camalexin Biosynthesis in Arabidopsis thaliana. Plant
937 Cell **23,** 364-380.
938 **Sun, Y., Li, H., and Huang, J.-R.** (2012). Arabidopsis TT19 Functions as a Carrier to Transport
939 Anthocyanin from the Cytosol to Tonoplasts. Molecular Plant **5,** 387-400.
940 **Tivendale, N.D., Ross, J.J., and Cohen, J.D.** (2014). The shifting paradigms of auxin biosynthesis. Trends
941 in Plant Science **19,** 44-51.
942 **Toufighi, K., Brady, S.M., Austin, R., Ly, E., and Provart, N.J.** (2005). The botany array resource: e-
943 northerns, expression angling, and promoter analyses. The Plant Journal **43,** 153-163.
944 **Tusher, V.G., Tibshirani, R., and Chu, G.** (2001). Significance analysis of microarrays applied to the
945 ionizing radiation response. Proceedings of the National Academy of Sciences **98,** 5116-5121.
946 **Tyanova, S., and Cox, J.** (2018). Perseus: A Bioinformatics Platform for Integrative Analysis of Proteomics
947 Data in Cancer Research. In Cancer Systems Biology (Springer), pp. 133-148.
948 **Vizcaíno, J.A., Côté, R.G., Csordas, A., Dianes, J.A., Fabregat, A., Foster, J.M., Griss, J., Alpi, E., Birim, M.,**
949 **and Contell, J.** (2012). The PRoteomics IDEntifications (PRIDE) database and associated tools: status in
950 2013. Nucleic Acids Research **41,** D1063-D1069.
951 **Wagner, U., Edwards, R., Dixon, D.P., and Mauch, F.** (2002). Probing the diversity of the Arabidopsis
952 glutathione S-transferase gene family. Plant Molecular Biology **49,** 515-532.
953 **Xu, J., Li, Y., Wang, Y., Liu, H., Lei, L., Yang, H., Liu, G., and Ren, D.** (2008). Activation of MAPK kinase 9
954 induces ethylene and camalexin biosynthesis and enhances sensitivity to salt stress in Arabidopsis.
955 Journal of Biological Chemistry **283,** 26996-27006.
956 **Zhao, Y., Hull, A.K., Gupta, N.R., Goss, K.A., Alonso, J., Ecker, J.R., Normanly, J., Chory, J., and Celenza,**
957 **J.L.** (2002). Trp-dependent auxin biosynthesis in Arabidopsis: involvement of cytochrome P450s CYP79B2
958 and CYP79B3. Genes & Development **16,** 3100-3112.
959 **Zhou, N., Tootle, T.L., and Glazebrook, J.** (1999). Arabidopsis PAD3, a gene required for camalexin
960 biosynthesis, encodes a putative cytochrome P450 monooxygenase. The Plant Cell **11,** 2419-2428.
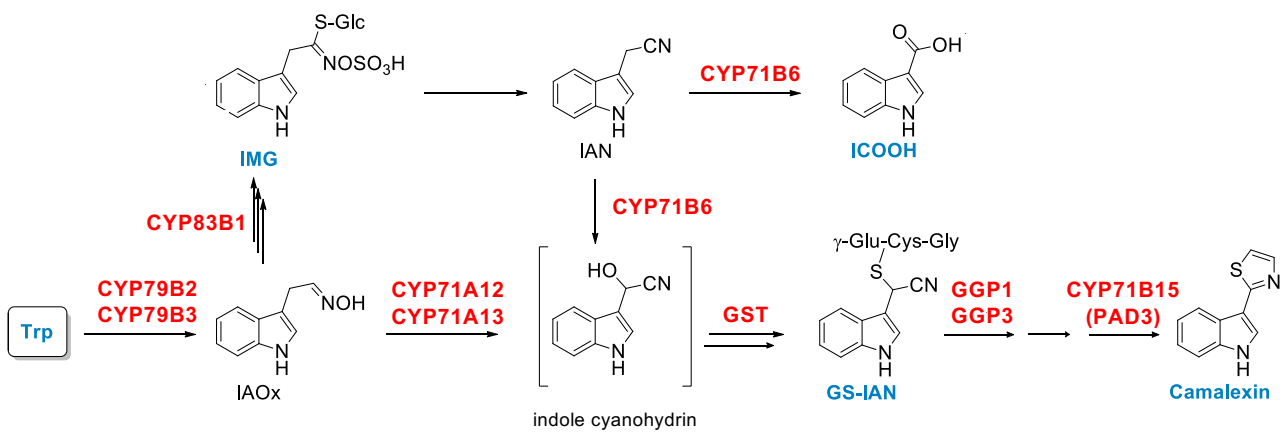961

Figure 1: Biosynthetic pathway of camalexin and related metabolites
Enzymes are marked in red, detected compounds are labeled in blue and biosynthetic intermediates in black; IMG: indole-3-methylglucosinolate; IAOx: indole-3-acetaldoxime; IAN: indole-3-acetonitrile; GS-IAN: IAN glutathione conjugate; ICOOH: indole-3-carboxylic acid.
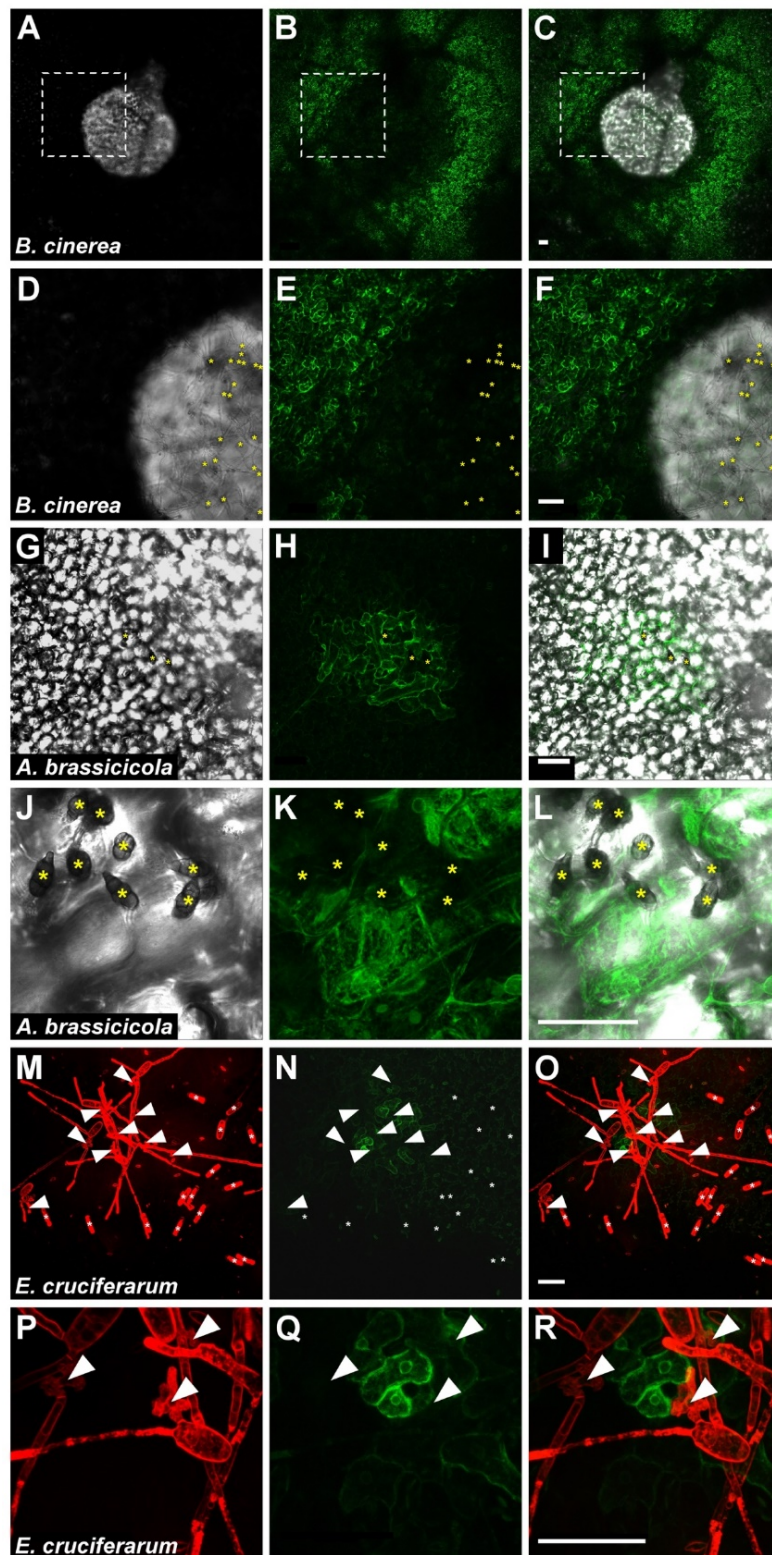
Figure 2: CYP71B15-GFP accumulates in cells surrounding fungal infection sites.

CYP71B15pro:CYP71B15-GFP expressing plants were inoculated with spores of *B. cinerea*, *A. brassicicola*, or *E. cruciferarum*, and expression of CYP71B15-GFP at fungal infections sites was detected. A-C: Site of infection with nectrotrophic *B. cinerea* (central transparent leaf area) 24 hai. D-F: Higher magnification of the area indicated by the square in A-C. Asterisks indicate spores from which hyphae emerged. G-L: Sites of infection with *A. brassicicola* 18 hai. Asterisks indicate spores from which hyphae emerged. M-R: Sites of successful infection by the biotrophic powdery mildew fungus *E. cruciferarum* 24 hai. Arrowheads indicate sites of fungal attack/penetration; asterisks indicate non-germinated spores. The first column of pictures shows transmission channel images (A, D, G, J) or red staining of fungal structures after staining with FM4-64 (M, P), images in the second column show CYP71B15-GFP accumulation, and the third columns shows the overlay images of the two. Bars = 50 μm.
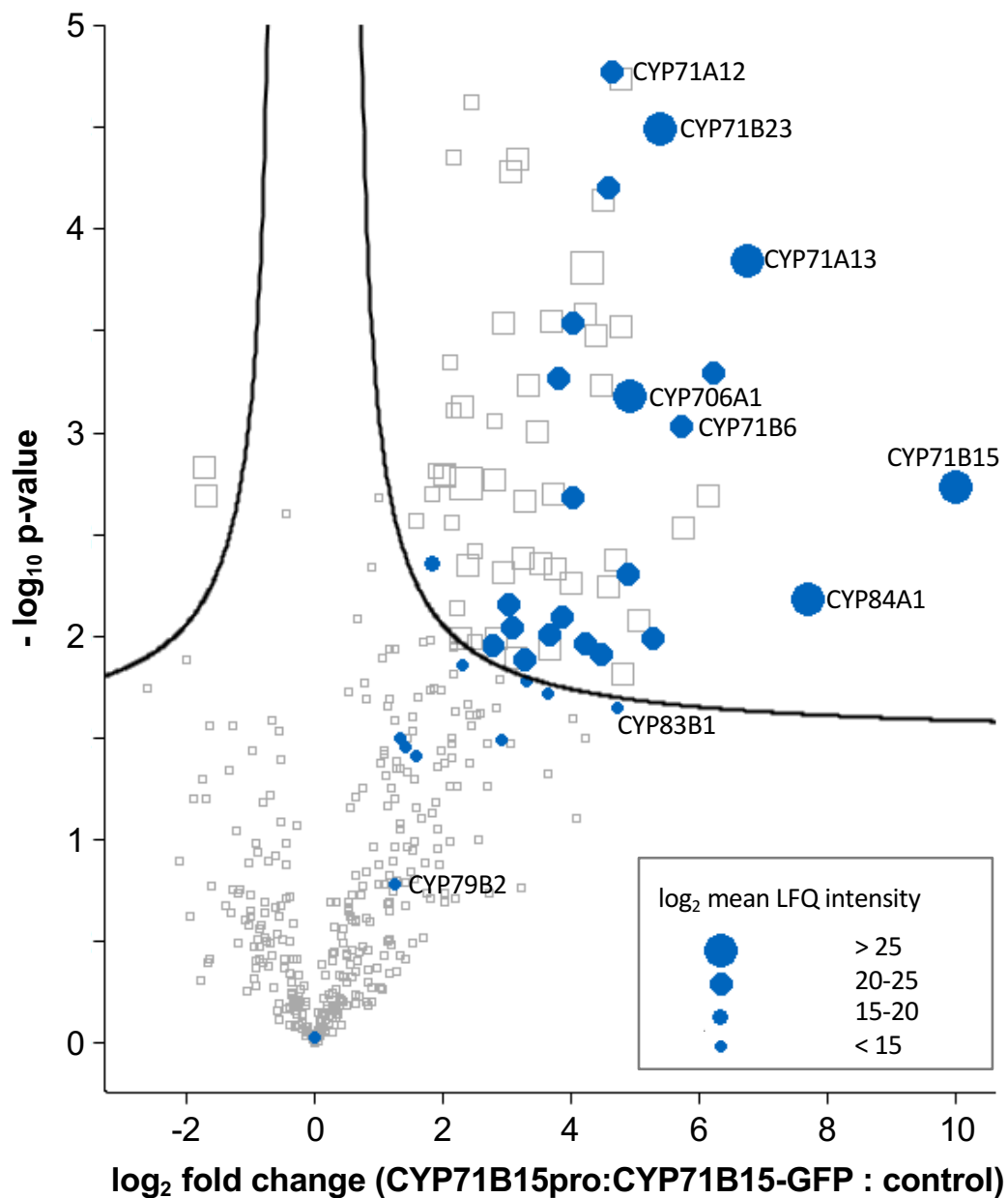
Figure 3: Proteins co-purified with CYP71B15-GFP from leaves infected with *B. cinerea*

CYP71B15-GFP was expressed under control of its endogenous promoter in the *pad3* background. The enrichment of interacting proteins in co-IP experiments ($\log_2$ fold change) is plotted against the significance of the change ($-\log_{10}$ p-value). Cytochrome P450 enzymes, represented by blue circles, all other proteins by open squares and there respective size represents $\log_2$ Label-free quantification intensities (LFQ). P450 enzymes were strongly enriched including CYP71A13 and CYP71B6. P450 proteins above $\log_2$ LFQ intensity of 25 and those mentioned in the text are indicated. n=3.
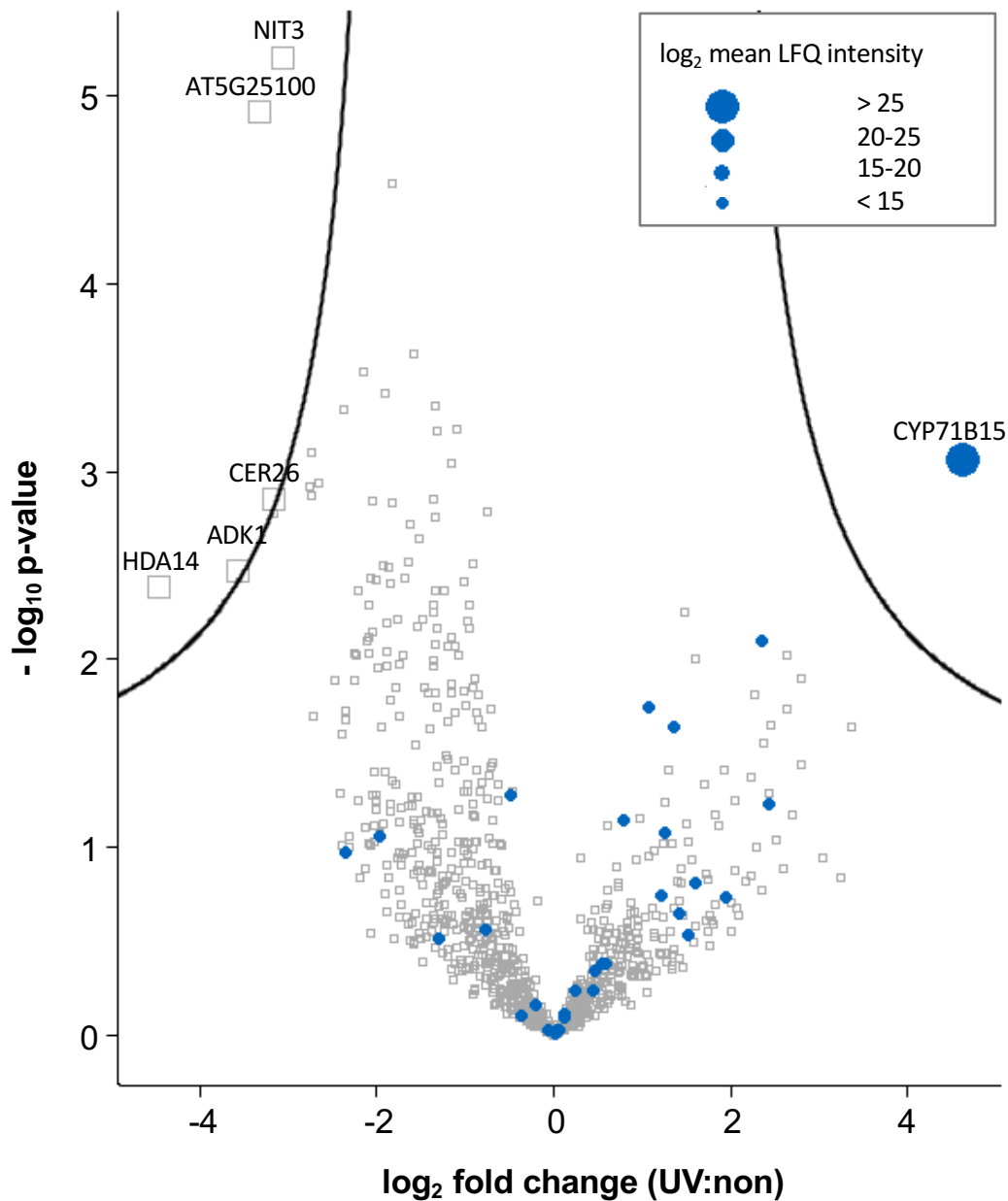
Figure 4: Proteins co-purified from leaves overexpressing CYP71A13-YFP with or without UV irradiation

The $\log_2$ fold change (UV-irradiated versus untreated leaves) is plotted against the significance of the change ($-\log_{10}$ p-value). Cytochrome P450 enzymes, represented by blue circles, all other proteins by open squares and there respective size represents $\log_2$ Label-free quantification intensities (LFQ). Named are proteins enriched significantly in UV or in control samples. UV-dependent co-purification of CYP71B15 was observed. n=3.
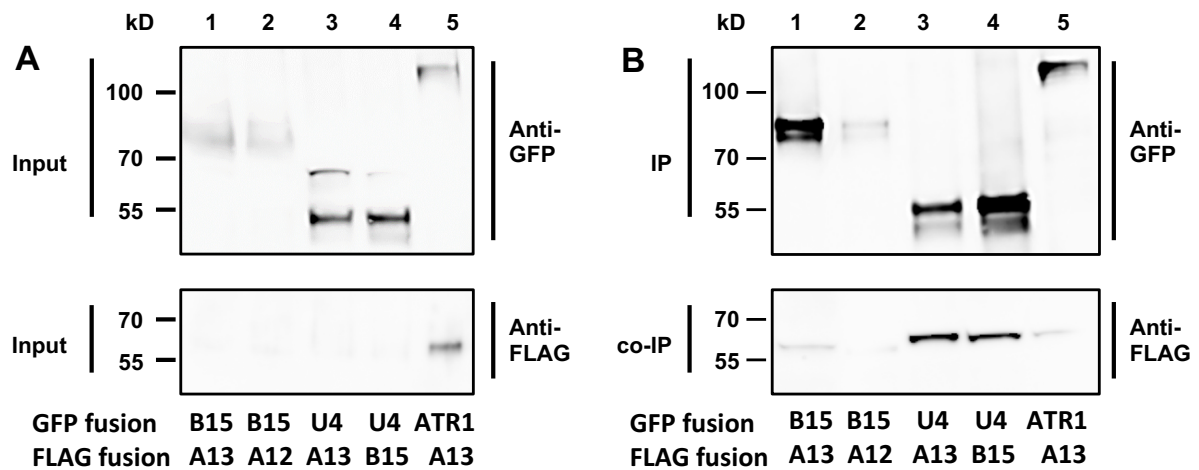
Figure 5: Co-IP analysis of the physical association of camalexin-specific enzymes

YFP and FLAG-tagged fusion proteins were transiently expressed in *N. benthamiana* and microsomal proteins were extracted four days after infiltration. Here, CYP71B15 (B15) in combination with CYP71A13 (A13) (1), CYP71A12 (A12) (2) or GSTU4 (U4) (4) and CYP71A13 in combination with GSTU4 (3) or ATR1 (5) **A**: Western blot analysis of input samples. **B:** Western Blot analysis on immunoprecipitation (IP) samples. IP was performed with anti-GFP antibody and interacting proteins were analysed with an anti-FLAG antibody. Interaction was shown for CYP71A13-FLAG with CYP71B15-YFP (1), GSTU4-YFP(3) and ATR1-YFP (5) and for CYP71B15-YFP with CYP71A12-FLAG (2) and GSTU4-FLAG (4). The experiment was repeated at least three times, with similar results. Combinations of fusion proteins, where no co-IP was observed are shown in Supplementary Figure 3.
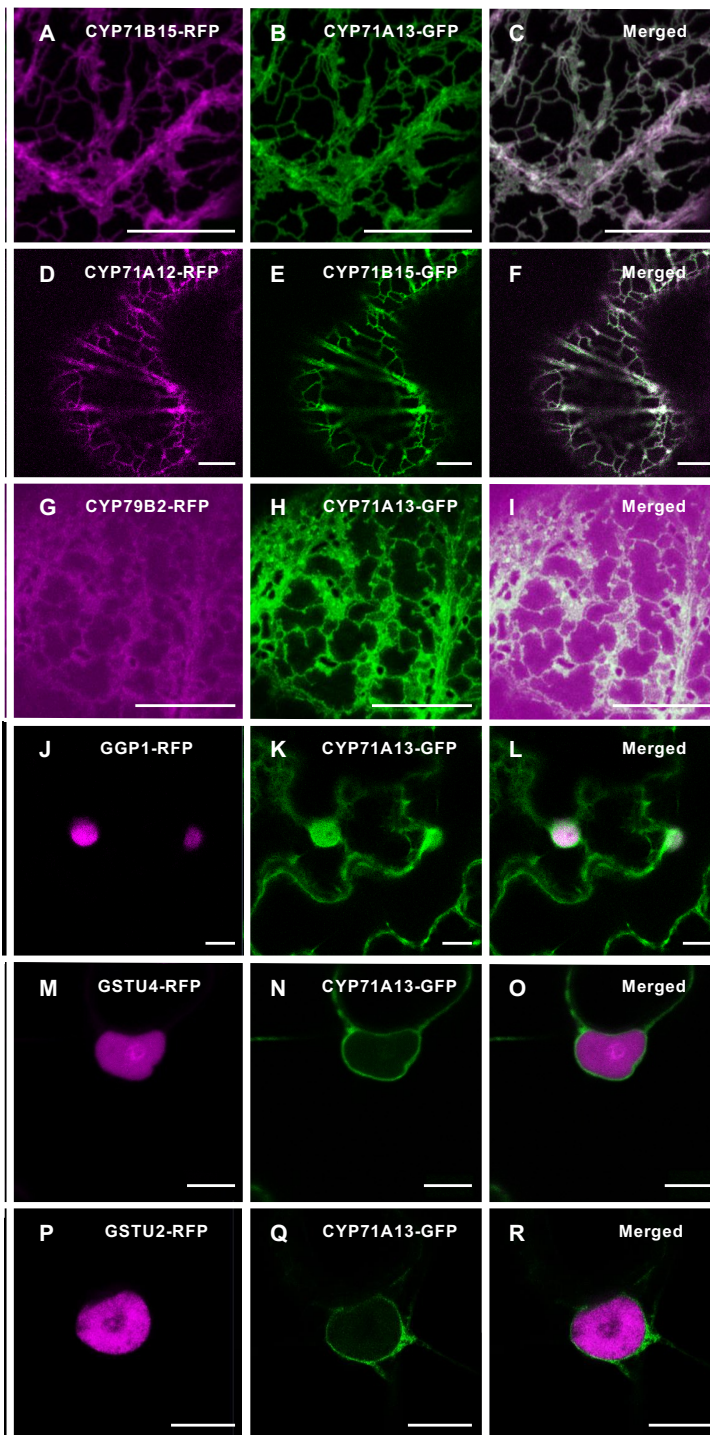
Figure 6: Co-localization of camalexin-specific enzymes in *N. benthamiana* leaves
In each case two GFP or RFP labelled P450 enzymes (A, B, D, E, G, H, K, N, Q) in different combinations or together with either GGP1-RFP (J), GSTU4-RFP (M) or GSTU2-RFP (P) were expressed transiently in *N. benthamiana* and analyzed for localization and co-localization three days after infiltration. Fluorescence signals for CYP71B15, CYP71A13, CYP71A12 and CYP79B2 fusion proteins were detected at the ER (A, B, D, E, G, H) with CYP79B2 expression levels substantially lower than the other proteins (G). GSTU4 (M) and GSTU2 (P) showed cytosolic localization indicated by the typical nuclear localization. Co-localization for CYP71A13 with CYP71B15 (C) and CYP79B2 (I) is shown in the merged images. Furthermore, CYP71B15 co-localizes with CYP71A12 (F) whereas no signal overlap is detectable when CYP71A13 is co-expressed with the cytosolic proteins GSTU4 (O) or GSTU2 (R) (see also Supplementary Fig. 4). Scale bar: 10 µm
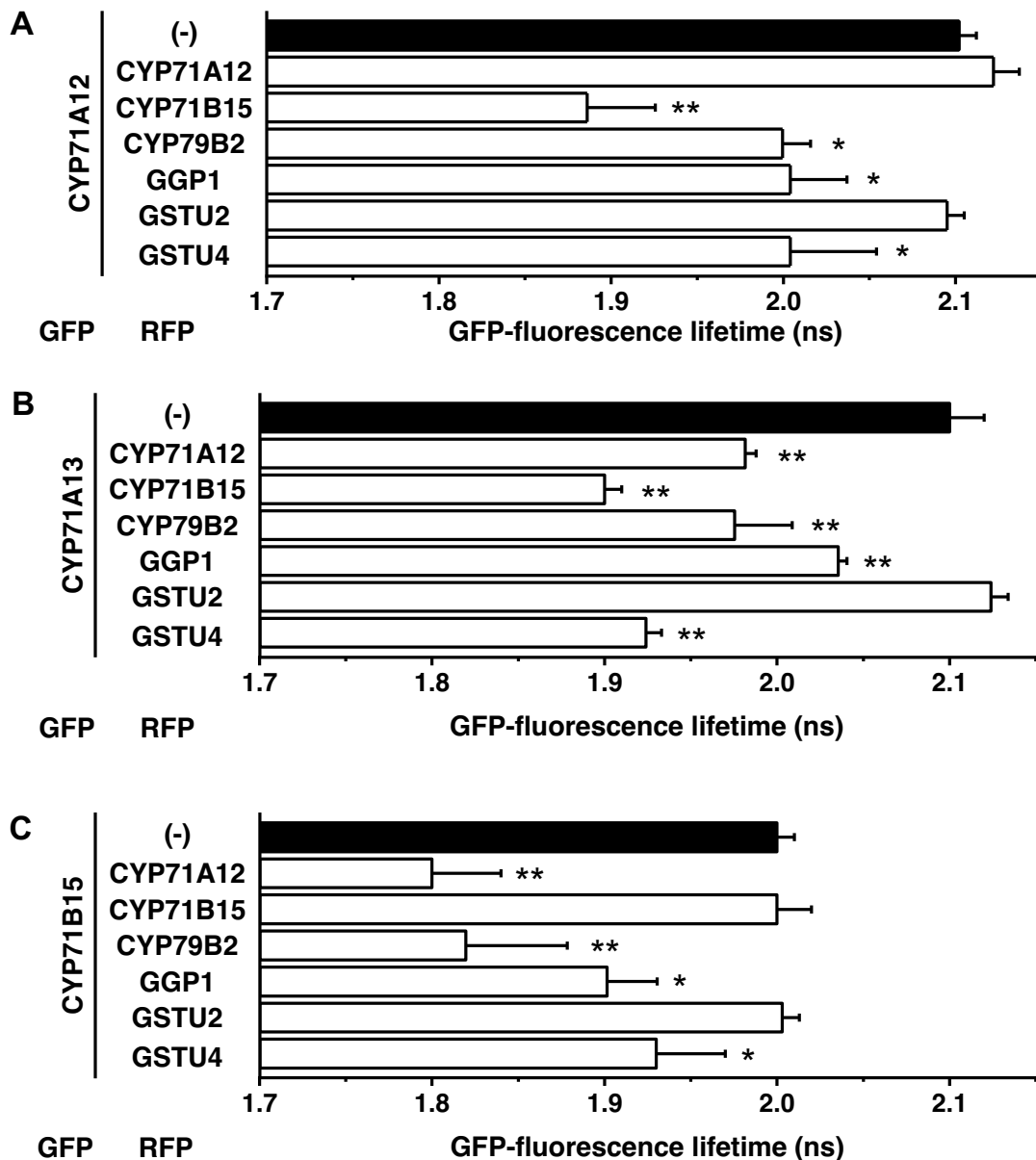
Figure 7: Tight physical interaction of camalexin-biosynthesis enzymes supported by Förster resonance energy transfer studies combined with fluorescence lifetime microscopy (FRET-FLIM)

GFP-tagged CYP71A12 (A), CYP71A13 (B) or CYP71B15 (C) was transiently expressed in *N. benthamiana* alone (black bars), or in combination with different RFP-tagged proteins (white bars). Three days after inoculation protein-protein interaction was determined by measuring the GFP-fluorescence lifetime via FLIM. In case of FRET a significant reduction of GFP-fluorescence lifetime was detectable compared to the donor only sample. Physical interaction could be observed for CYP71A12, CYP71A13, CYP71B15 with each other and with CYP79B2, GGP1, and GSTU4. No interaction with GSTU2 and no homodimerization of CYP71A12 or CYP71B15 was observed. Error bars indicate standard deviation of at least three independent replicates. One-way Anova for independent samples, standard weighted-means analysis, with Tukey's honestly significant difference (HSD) post hoc test; *p<0.05; **p<0.01.
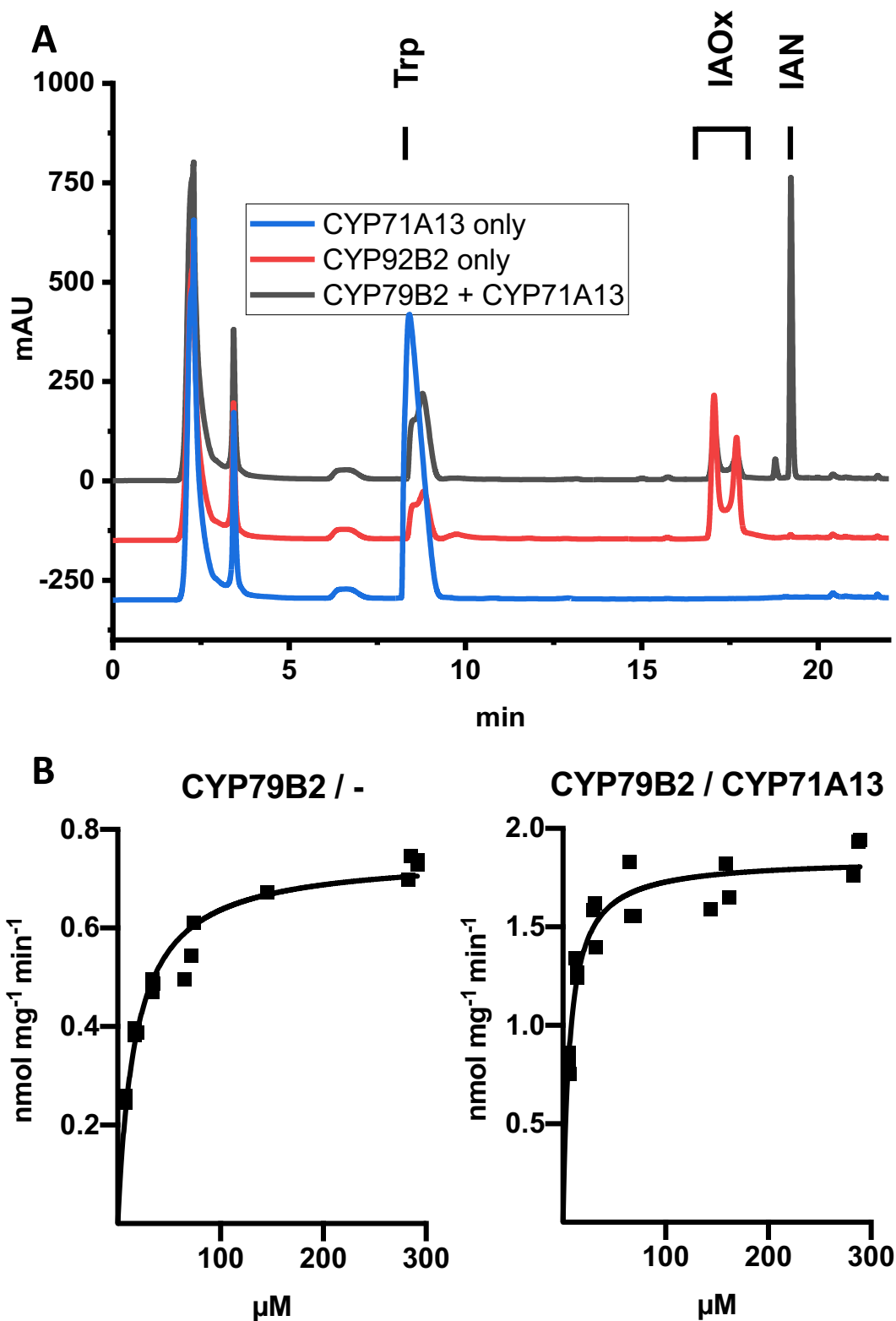
Figure 8: Higher apparent substrate affinity of CYP79B2 by presence of CYP71A13

CYP79B2 was expressed in *S. cerevisiae* together with CYP71A13 or vector control. **A:** Turnover of tryptophan with NADPH as co-substrate by corresponding microsomes; detection of substrate and products by HPLC; chromatogram at 278 nm. **B**: app. Km-value for tryptophan: CYP79B2: Km=17.5 ± 1.9 μM, R^2=0.95; CYP79B2 / CYP71B13: Km=6.9 ± 0.9 μM, R^2=0.90 (n=16).
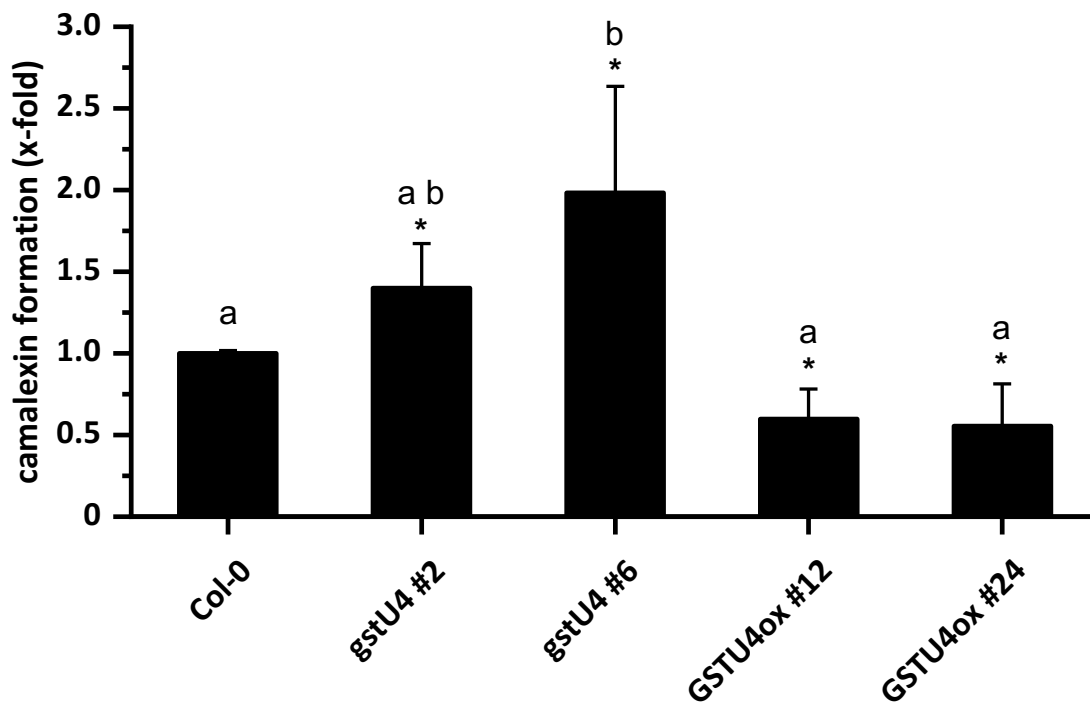
Figure 9: Camalexin formation in response to *B. cinerea* infection in *gstu4* knockout and overexpression plants

Leaves of six-week-old plants were treated with *B. cinerea* spores. After 48 hours camalexin was extracted and levels were analyzed via HPLC. In *gstu4* lines camalexin level was significantly increased whereas a significant decrease was observed in GSTU4 overexpressing lines. Camalexin levels were shown as arithmetic mean with standard deviation of 27 independent plants Different letters indicate significant differences according to ANOVA (Scheffé's test; $P < 0.05$); *: significant differences to Col-0 according to t-test ($P < 0.05$).
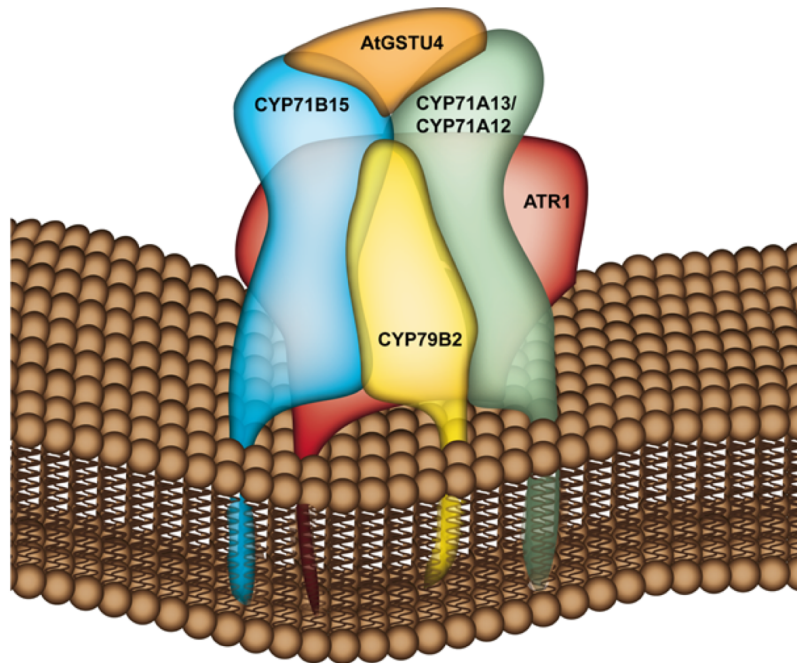
Figure 10: Model of a camalexin-biosynthetic metabolon

CYP79B2, CYP71A12/A13, CYP71B15 and ATR1 form a metabolic complex at the ER surface. CYP71B15 interacts with CYP79B2, CYP71A13 and CYP71A12 respectively. CYP79B2 is rather loosely associated to the complex and might function as a branch-point enzyme taking part in different protein complexes. Under stress conditions, the cytosolic component GSTU4 might be recruited to the complex. Its role in camalexin biosynthesis remains unsettled.

Parsed Citations

Adler, V., Yin, Z, Fuchs, S.Y., Benezra, M., Rosario, L., Tew, K.D., Pincus, M.R., Sardana, M., Henderson, C.J., and Wolf, C.R. (1999). Regulation of JNK signaling by GSTp. The EMBO journal 18, 1321-1334.
Pubmed: Author and Title
Google Scholar: Author Only Title Only Author and Title

Amberg, D.C., Burke, D.J., and Strathern, J.N. (2005). Methods in Yeast Genetics: A Cold Spring Harbor Laboratory Course Manual, 2005 Edition (Cold Spring).

Bak, S., Tax, F.E., Feldmann, K.A, Galbraith, D.W., and Feyereisen, R. (2001). CYP83B1, a cytochrome P450 at the metabolic branch point in auxin and indole glucosinolate biosynthesis in Arabidopsis. The Plant Cell 13, 101-111.
Pubmed: Author and Title
Google Scholar: Author Only Title Only Author and Title

Bak, S., Beisson, F., Bishop, G., Hamberger, B., Höfer, R., Paquette, S., and Werck-Reichhart, D. (2011). Cytochromes P450. The Arabidopsis Book, e0144.
Pubmed: Author and Title
Google Scholar: Author Only Title Only Author and Title

Bassard, J.E., Richert, L., Geerinck, J., Renault, H., Duval, F., Ullmann, P., Schmitt, M., Meyer, E., Mutterer, J., Boerjan, W., De Jaeger, G., Mely, Y., Goossens, A, and Werck-Reichhart, D. (2012). Protein-protein and protein-membrane associations in the lignin pathway. Plant Cell 24, 4465-4482.
Pubmed: Author and Title
Google Scholar: Author Only Title Only Author and Title

Becker, D., Kemper, E., Schell, J., and Masterson, R. (1992). New plant binary vectors with selectable markers located proximal to the left T-DNA border. Plant Molecular Biology 20, 1195-1197.
Pubmed: Author and Title
Google Scholar: Author Only Title Only Author and Title

Becker, W. (2012). Fluorescence lifetime imaging–techniques and applications. Journal of Microscopy 247, 119-136.
Pubmed: Author and Title
Google Scholar: Author Only Title Only Author and Title

Bednarek, P., Schneider, B., Svatoš, A, Oldham, N.J., and Hahlbrock, K. (2005). Structural complexity, differential response to infection, and tissue specificity of indolic and phenylpropanoid secondary metabolism in Arabidopsis roots. Plant Physiology 138, 1058-1070.
Pubmed: Author and Title
Google Scholar: Author Only Title Only Author and Title

Böttcher, C., Westphal, L., Schmotz, C., Prade, E., Scheel, D., and Glawischnig, E. (2009). The multifunctional enzyme CYP71B15 (PHYTOALEXIN DEFICIENT3) converts cysteine-indole-3-acetonitrile to camalexin in the indole-3-acetonitrile metabolic network of Arabidopsis thaliana. Plant Cell 21, 1830-1845.
Pubmed: Author and Title
Google Scholar: Author Only Title Only Author and Title

Böttcher, C., Chapman, A, Fellermeier, F., Choudhary, M., Scheel, D., and Glawischnig, E. (2014). The Biosynthetic Pathway of Indole-3-Carbaldehyde and Indole-3-Carboxylic Acid Derivatives in Arabidopsis. Plant Physiol 165, 841-853.
Pubmed: Author and Title
Google Scholar: Author Only Title Only Author and Title

Brachmann, C.B., Davies, A, Cost, G.J., Caputo, E., Li, J., Hieter, P., and Boeke, J.D. (1998). Designer deletion strains derived from Saccharomyces cerevisiae S288C: a useful set of strains and plasmids for PCR-mediated gene disruption and other applications. Yeast 14, 115-132.
Pubmed: Author and Title
Google Scholar: Author Only Title Only Author and Title

Brumos, J., Alonso, J.M., and Stepanova, A.N. (2014). Genetic aspects of auxin biosynthesis and its regulation. Physiologia Plantarum 151, 3-12.
Pubmed: Author and Title
Google Scholar: Author Only Title Only Author and Title

Chapman, A, Lindermayr, C., and Glawischnig, E. (2016). Expression of antimicrobial peptides under control of a camalexin-biosynthetic promoter confers enhanced resistance against Pseudomonas syringae. Phytochemistry 122, 76-80.
Pubmed: Author and Title
Google Scholar: Author Only Title Only Author and Title

Clough, S.J., and Bent, A.F. (1998). Floral dip: a simplified method for Agrobacterium-mediated transformation of Arabidopsis thaliana. Plant Journal 16, 735-743.
Pubmed: Author and Title
Google Scholar: Author Only Title Only Author and Title

Cobbett, C.S., May, M.J., Howden, R., and Rolls, B. (1998). The glutathione-deficient, cadmium-sensitive mutant, cad2-1, of Arabidopsis

thaliana is deficient in gamma-glutamylcysteine synthetase. Plant J 16, 73-78.
Pubmed: Author and Title
Google Scholar: Author Only Title Only Author and Title

Cox, J., and Mann, M. (2008). MaxQuant enables high peptide identification rates, individualized ppb-range mass accuracies and proteome-wide protein quantification. Nature Biotechnology 26, 1367.
Pubmed: Author and Title
Google Scholar: Author Only Title Only Author and Title

Cox, J., Neuhauser, N., Michalski, A, Scheltema, R.A, Olsen, J.V., and Mann, M. (2011). Andromeda: a peptide search engine integrated into the MaxQuant environment. Journal of Proteome Research 10, 1794-1805.
Pubmed: Author and Title
Google Scholar: Author Only Title Only Author and Title

Cox, J., Hein, M.Y., Luber, C.A, Paron, I., Nagaraj, N., and Mann, M. (2014). Accurate Proteome-wide Label-free Quantification by Delayed Normalization and Maximal Peptide Ratio Extraction, Termed MaxLFQ. Molecular & Cellular Proteomics 13, 2513-2526.
Pubmed: Author and Title
Google Scholar: Author Only Title Only Author and Title

Crosby, K.C., Pietraszewska-Bogiel, A, Gadella, T.W., Jr., and Winkel, B.S. (2011). Forster resonance energy transfer demonstrates a flavonoid metabolon in living plant cells that displays competitive interactions between enzymes. FEBS Letters 585, 2193-2198.
Pubmed: Author and Title
Google Scholar: Author Only Title Only Author and Title

Czerniawski, P., and Bednarek, P. (2018). Glutathione S-Transferases in the Biosynthesis of Sulfur-Containing Secondary Metabolites in Brassicaceae Plants. Front Plant Sci 9, 1639.
Pubmed: Author and Title
Google Scholar: Author Only Title Only Author and Title

Dastmalchi, M., Bernards, M.A, and Dhaubhadel, S. (2016). Twin anchors of the soybean isoflavonoid metabolon: evidence for tethering of the complex to the endoplasmic reticulum by IFS and C4H. The Plant Journal 85, 689-706.
Pubmed: Author and Title
Google Scholar: Author Only Title Only Author and Title

Davydov, D.R., Davydova, N.Y., Sineva, E.V., and Halpert, J.R. (2015). Interactions among cytochromes P450 in microsomal membranes: oligomerization of cytochromes P450 3A4, 3A5, and 2E1 and its functional consequences. Journal of Biological Chemistry 290, 3850-3864.
Pubmed: Author and Title
Google Scholar: Author Only Title Only Author and Title

Dixon, D.P., Lapthorn, A, and Edwards, R. (2002). Plant glutathione transferases. Genome Biology 3, reviews3004. 3001.
Pubmed: Author and Title
Google Scholar: Author Only Title Only Author and Title

Förster, T. (1948). Zwischenmolekulare Energiewanderung und Fluoreszenz. Annalen der Physik 437, 55-75.
Pubmed: Author and Title
Google Scholar: Author Only Title Only Author and Title

Frerigmann, H., Pislewska-Bednarek, M., Sanchez-Vallet, A, Molina, A, Glawischnig, E., Gigolashvili, T., and Bednarek, P. (2016). Regulation of Pathogen-Triggered Tryptophan Metabolism in Arabidopsis thaliana by MYB Transcription Factors and Indole Glucosinolate Conversion Products. Mol Plant 9, 682-695.
Pubmed: Author and Title
Google Scholar: Author Only Title Only Author and Title

Fuchs, R., Kopischke, M., Klapprodt, C., Hause, G., Meyer, A.J., Schwarzlander, M., Fricker, M.D., and Lipka, V. (2016). Immobilized Subpopulations of Leaf Epidermal Mitochondria Mediate PENETRATION2-Dependent Pathogen Entry Control in Arabidopsis. The Plant cell 28, 130-145.
Pubmed: Author and Title
Google Scholar: Author Only Title Only Author and Title

Fujino, N., Tenma, N., Waki, T., Ito, K., Komatsuzaki, Y., Sugiyama, K., Yamazaki, T., Yoshida, S., Hatayama, M., Yamashita, S., Tanaka, Y., Motohashi, R., Denessiouk, K., Takahashi, S., and Nakayama, T. (2018). Physical interactions among flavonoid enzymes in snapdragon and torenia reveal the diversity in the flavonoid metabolon organization of different plant species. Plant J 94, 372-392.
Pubmed: Author and Title
Google Scholar: Author Only Title Only Author and Title

Gietz, D., St Jean, A, Woods, R.A, and Schiestl, R.H. (1992). Improved method for high efficiency transformation of intact yeast cells. Nucleic Acids Research 20, 1425.
Pubmed: Author and Title
Google Scholar: Author Only Title Only Author and Title

Glawischnig, E., Hansen, B.G., Olsen, C.E., and Halkier, B.A. (2004). Camalexin is synthesized from indole-3-acetaldoxime, a key branching point between primary and secondary metabolism in Arabidopsis. Proceedings of the National Academy of Sciences 101, 8245-8250.

Pubmed: Author and Title
Google Scholar: Author Only Title Only Author and Title

Glazebrook, J., and Ausubel, F.M. (1994). Isolation of phytoalexin-deficient mutants of Arabidopsis thaliana and characterization of their interactions with bacterial pathogens. Proceedings of the National Academy of Sciences 91, 8955-8959.
Pubmed: Author and Title
Google Scholar: Author Only Title Only Author and Title

Gronover, C.S., Kasulke, D., Tudzynski, P., and Tudzynski, B. (2001). The role of G protein alpha subunits in the infection process of the gray mold fungus Botrytis cinerea. Mol Plant Microbe Interact 14, 1293-1302.
Pubmed: Author and Title
Google Scholar: Author Only Title Only Author and Title

Hansen, C.H., Du, L., Naur, P., Olsen, C.E., Axelsen, K.B., Hick, A.J., Pickett, J.A., and Halkier, B.A. (2001). CYP83B1 is the oxime-metabolizing enzyme in the glucosinolate pathway in Arabidopsis. Journal of Biological Chemistry 276, 24790-24796.
Pubmed: Author and Title
Google Scholar: Author Only Title Only Author and Title

Hawes, C., and Kriechbaumer, V. (2018). The Plant Endoplasmic Reticulum. (Springer).
Pubmed: Author and Title
Google Scholar: Author Only Title Only Author and Title

He, Y., Xu, J., Wang, X., He, X., Wang, Y., Zhou, J., Zhang, S., and Meng, X. (2019). The Arabidopsis Pleiotropic Drug Resistance Transporters PEN3 and PDR12 Mediate Camalexin Secretion for Resistance to Botrytis cinerea. The Plant cell.
Pubmed: Author and Title
Google Scholar: Author Only Title Only Author and Title

Julkowska, M., Koevoets, I.T., Mol, S., Hoefsloot, H.C., Feron, R., Tester, M., Keurentjes, J.J., Korte, A., Haring, M.A., and de Boer, G.-J. (2017). Genetic Components of Root Architecture Remodeling in Response to Salt Stress. The Plant Cell, tpc. 00680.02016.
Pubmed: Author and Title
Google Scholar: Author Only Title Only Author and Title

Karimi, M., De Meyer, B., and Hilson, P. (2005). Modular cloning in plant cells. Trends in Plant Science 10, 103-105.
Pubmed: Author and Title
Google Scholar: Author Only Title Only Author and Title

Katzen, F. (2007). Gateway® recombinational cloning: a biological operating system. Expert Opinion on Drug Discovery 2, 571-589.
Pubmed: Author and Title
Google Scholar: Author Only Title Only Author and Title

Kitamura, S., Shikazono, N., and Tanaka, A. (2004). TRANSPARENT TESTA 19 is involved in the accumulation of both anthocyanins and proanthocyanidins in Arabidopsis. The Plant Journal 37, 104-114.
Pubmed: Author and Title
Google Scholar: Author Only Title Only Author and Title

Klein, A.P., Anarat-Cappillino, G., and Sattely, E.S. (2013). Minimum Set of Cytochromes P450 for Reconstituting the Biosynthesis of Camalexin, a Major Arabidopsis Antibiotic. Angewandte Chemie International Edition 52, 13625-13628.
Pubmed: Author and Title
Google Scholar: Author Only Title Only Author and Title

Knudsen, C., Gallage, N.J., Hansen, C.C., Moller, B.L., and Laursen, T. (2018). Dynamic metabolic solutions to the sessile life style of plants. Nat Prod Rep 35, 1140-1155.
Pubmed: Author and Title
Google Scholar: Author Only Title Only Author and Title

Kowalski, N.A. (2016). Charakterisierung der Glutathiontransferasen aus Arabidopsis thaliana. In Fakultät Wissenschaftszentrum Weihenstephan (Freising: TU-München), pp. 216.
Pubmed: Author and Title
Google Scholar: Author Only Title Only Author and Title

Krajewski, M.P., Kanawati, B., Fekete, A., Kowalski, N., Schmitt-Kopplin, P., and Grill, E. (2013). Analysis of Arabidopsis glutathione-transferases in yeast. Phytochemistry 91, 198-207.
Pubmed: Author and Title
Google Scholar: Author Only Title Only Author and Title

Kriechbaumer, V., Botchway, S.W., Slade, S.E., Knox, K., Frigerio, L., Oparka, K., and Hawes, C. (2015). Reticulomics: Protein-Protein Interaction Studies with Two Plasmodesmata-Localized Reticulon Family Proteins Identify Binding Partners Enriched at Plasmodesmata, Endoplasmic Reticulum, and the Plasma Membrane. Plant Physiology 169, 1933-1945.
Pubmed: Author and Title
Google Scholar: Author Only Title Only Author and Title

Kutz, A., Müller, A., Hennig, P., Kaiser, W.M., Piotrowski, M., and Weiler, E.W. (2002). A role for nitrilase 3 in the regulation of root morphology in sulphur-starving Arabidopsis thaliana. The Plant Journal 30, 95-106.
Pubmed: Author and Title
Google Scholar: Author Only Title Only Author and Title

Lallemand, B., Erhardt, M., Heitz, T., and Legrand, M. (2013). Sporopollenin biosynthetic enzymes interact and constitute a metabolon localized to the endoplasmic reticulum of tapetum cells. Plant physiology 162, 616-625.

Pubmed: Author and Title
Google Scholar: Author Only Title Only Author and Title

Laursen, T., Borch, J., Knudsen, C., Bavishi, K., Torta, F., Martens, H.J., Silvestro, D., Hatzakis, N.S., Wenk, M.R., and Dafforn, T.R. (2016). Characterization of a dynamic metabolon producing the defense compound dhurrin in sorghum. Science 354, 890-893.

Pubmed: Author and Title
Google Scholar: Author Only Title Only Author and Title

Lemarié, S., Robert-Seilaniantz, A, Lariagon, C., Lemoine, J., Marnet, N., Levrel, A, Jubault, M., Manzanares-Dauleux, M.J., and Gravot, A. (2015). Camalexin contributes to the partial resistance of Arabidopsis thaliana to the biotrophic soilborne protist Plasmodiophora brassicae. Frontiers in plant science 6.

Pubmed: Author and Title
Google Scholar: Author Only Title Only Author and Title

Mikkelsen, M.D., Hansen, C.H., Wittstock, U., and Halkier, B.A. (2000). Cytochrome P450 CYP79B2 from Arabidopsis catalyzes the conversion of tryptophan to indole-3-acetaldoxime, a precursor of indole glucosinolates and indole-3-acetic acid. Journal of Biological Chemistry 275, 33712-33717.

Pubmed: Author and Title
Google Scholar: Author Only Title Only Author and Title

Müller, T.M., Böttcher, C., and Glawischnig, E. (2019). Dissection of the network of indolic defence compounds in Arabidopsis thaliana by multiple mutant analysis. Phytochemistry 161, 11-20.

Pubmed: Author and Title
Google Scholar: Author Only Title Only Author and Title

Müller, T.M., Böttcher, C., Morbitzer, R., Götz, C.C., Lehmann, J., Lahaye, T., and Glawischnig, E. (2015). Transcription activator-like effector nuclease-mediated generation and metabolic analysis of camalexin-deficient cyp71a12 cyp71a13 double knockout lines. Plant Physiology 168, 849-858.

Pubmed: Author and Title
Google Scholar: Author Only Title Only Author and Title

Nafisi, M., Goregaoker, S., Botanga, C.J., Glawischnig, E., Olsen, C.E., Halkier, B.A, and Glazebrook, J. (2007). Arabidopsis cytochrome P450 monooxygenase 71A13 catalyzes the conversion of indole-3-acetaldoxime in camalexin synthesis. The Plant cell 19, 2039-2052.

Pubmed: Author and Title
Google Scholar: Author Only Title Only Author and Title

Nintemann, S.J., Vik, D., Svozil, J., Bak, M., Baerenfaller, K., Burow, M., and Halkier, B.A. (2017). Unravelling protein-protein interaction networks linked to aliphatic and indole glucosinolate biosynthetic pathways in Arabidopsis. Frontiers in Plant Science 8.

Pubmed: Author and Title
Google Scholar: Author Only Title Only Author and Title

Nirenberg, H.I. (1981). A simplified method for identifying Fusarium spp. occuring on wheat. Canadian Journal of Botany 59, 1599-1609.

Pubmed: Author and Title
Google Scholar: Author Only Title Only Author and Title

Parisy, V., Poinssot, B., Owsianowski, L., Buchala, A, Glazebrook, J., and Mauch, F. (2007). Identification of PAD2 as a γ-glutamylcysteine synthetase highlights the importance of glutathione in disease resistance of Arabidopsis. The Plant Journal 49, 159-172.

Pubmed: Author and Title
Google Scholar: Author Only Title Only Author and Title

Perkins, J.R., Diboun, I., Dessailly, B.H., Lees, J.G., and Orengo, C. (2010). Transient protein-protein interactions: structural, functional, and network properties. Structure 18, 1233-1243.

Pubmed: Author and Title
Google Scholar: Author Only Title Only Author and Title

Rajniak, J., Barco, B., Clay, N.K., and Sattely, E.S. (2015). A new cyanogenic metabolite in Arabidopsis required for inducible pathogen defence. Nature 525, 376-379.

Pubmed: Author and Title
Google Scholar: Author Only Title Only Author and Title

Rauhut, T. (2009). Die Regulation der Camalexinbiosynthese in Arabidopsis thaliana. In Lehrstuhl für Genetik (Freising: TU-München).

Pubmed: Author and Title
Google Scholar: Author Only Title Only Author and Title

Rauhut, T., and Glawischnig, E. (2009). Evolution of camalexin and structurally related indolic compounds. Phytochemistry 70, 1638-1644.

Pubmed: Author and Title
Google Scholar: Author Only Title Only Author and Title

Reed, J.R., and Backes, W.L. (2012). Formation of P450· P450 complexes and their effect on P450 function. Pharmacology & Therapeutics 133, 299-310.

Pubmed: Author and Title
Google Scholar: Author Only Title Only Author and Title

Rothbauer, U., Zolghadr, K., Muyldermans, S., Schepers, A., Cardoso, M.C., and Leonhardt, H. (2008). A versatile nanotrap for biochemical and functional studies with fluorescent fusion proteins. Molecular & Cellular Proteomics 7, 282-289.
Pubmed: Author and Title
Google Scholar: Author Only Title Only Author and Title

Schlaeppi, K., Abou-Mansour, E., Buchala, A., and Mauch, F. (2010). Disease resistance of Arabidopsis to Phytophthora brassicae is established by the sequential action of indole glucosinolates and camalexin. The Plant Journal 62, 840-851.
Pubmed: Author and Title
Google Scholar: Author Only Title Only Author and Title

Schoberer, J., and Botchway, S.W. (2014). Investigating protein-protein interactions in the plant endomembrane system using multiphoton-induced FRET-FLIM. Methods in Molecular Biology 1209, 81-95.
Pubmed: Author and Title
Google Scholar: Author Only Title Only Author and Title

Schuhegger, R., Nafisi, M., Mansourova, M., Petersen, B.L., Olsen, C.E., Svatos, A., Halkier, B.A., and Glawischnig, E. (2006). CYP71B15 (PAD3) catalyzes the final step in camalexin biosynthesis. Plant Physiology 141, 1248-1254.
Pubmed: Author and Title
Google Scholar: Author Only Title Only Author and Title

Shevchenko, A, Tomas, H., Havli, J., Olsen, J.V., and Mann, M. (2006). In-gel digestion for mass spectrometric characterization of proteins and proteomes. Nature Protocols 1, 2856.
Pubmed: Author and Title
Google Scholar: Author Only Title Only Author and Title

Sønderby, I.E., Geu-Flores, F., and Halkier, B.A (2010). Biosynthesis of glucosinolates–gene discovery and beyond. Trends in plant science 15, 283-290.
Pubmed: Author and Title
Google Scholar: Author Only Title Only Author and Title

Sparkes, I.A, Runions, J., Kearns, A, and Hawes, C. (2006). Rapid, transient expression of fluorescent fusion proteins in tobacco plants and generation of stably transformed plants. Nature Protocols 1, 2019-2025.
Pubmed: Author and Title
Google Scholar: Author Only Title Only Author and Title

Su, T.B., Xu, J.A, Li, Y.A, Lei, L., Zhao, L., Yang, H.L., Feng, J.D., Liu, G.Q., and Ren, D.T. (2011). Glutathione-Indole-3-Acetonitrile Is Required for Camalexin Biosynthesis in Arabidopsis thaliana. Plant Cell 23, 364-380.
Pubmed: Author and Title
Google Scholar: Author Only Title Only Author and Title

Sun, Y., Li, H., and Huang, J.-R. (2012). Arabidopsis TT19 Functions as a Carrier to Transport Anthocyanin from the Cytosol to Tonoplasts. Molecular Plant 5, 387-400.
Pubmed: Author and Title
Google Scholar: Author Only Title Only Author and Title

Tivendale, N.D., Ross, J.J., and Cohen, J.D. (2014). The shifting paradigms of auxin biosynthesis. Trends in Plant Science 19, 44-51.
Pubmed: Author and Title
Google Scholar: Author Only Title Only Author and Title

Toufighi, K., Brady, S.M., Austin, R., Ly, E., and Provart, N.J. (2005). The botany array resource: e-northerns, expression angling, and promoter analyses. The Plant Journal 43, 153-163.
Pubmed: Author and Title
Google Scholar: Author Only Title Only Author and Title

Tusher, V.G., Tibshirani, R., and Chu, G. (2001). Significance analysis of microarrays applied to the ionizing radiation response. Proceedings of the National Academy of Sciences 98, 5116-5121.
Pubmed: Author and Title
Google Scholar: Author Only Title Only Author and Title

Tyanova, S., and Cox, J. (2018). Perseus: A Bioinformatics Platform for Integrative Analysis of Proteomics Data in Cancer Research. In Cancer Systems Biology (Springer), pp. 133-148.
Pubmed: Author and Title
Google Scholar: Author Only Title Only Author and Title

Vizcaíno, J.A, Côté, R.G., Csordas, A, Dianes, J.A, Fabregat, A, Foster, J.M., Griss, J., Alpi, E., Birim, M., and Contell, J. (2012). The PRoteomics IDEntifications (PRIDE) database and associated tools: status in 2013. Nucleic Acids Research 41, D1063-D1069.
Pubmed: Author and Title
Google Scholar: Author Only Title Only Author and Title

Wagner, U., Edwards, R., Dixon, D.P., and Mauch, F. (2002). Probing the diversity of the Arabidopsis glutathione S-transferase gene family. Plant Molecular Biology 49, 515-532.
Pubmed: Author and Title

Google Scholar: [Author Only](#) [Title Only](#) [Author and Title](#)

Xu, J., Li, Y., Wang, Y., Liu, H., Lei, L., Yang, H., Liu, G., and Ren, D. (2008). Activation of MAPK kinase 9 induces ethylene and camalexin biosynthesis and enhances sensitivity to salt stress in Arabidopsis. Journal of Biological Chemistry 283, 26996-27006.

Pubmed: [Author and Title](#)
Google Scholar: [Author Only](#) [Title Only](#) [Author and Title](#)

Zhao, Y., Hull, A.K., Gupta, N.R., Goss, K.A, Alonso, J., Ecker, J.R., Normanly, J., Chory, J., and Celenza, J.L. (2002). Trp-dependent auxin biosynthesis in Arabidopsis: involvement of cytochrome P450s CYP79B2 and CYP79B3. Genes & Development 16, 3100-3112.

Pubmed: [Author and Title](#)
Google Scholar: [Author Only](#) [Title Only](#) [Author and Title](#)

Zhou, N., Tootle, T.L., and Glazebrook, J. (1999). Arabidopsis PAD3, a gene required for camalexin biosynthesis, encodes a putative cytochrome P450 monooxygenase. The Plant Cell 11, 2419-2428.

Pubmed: [Author and Title](#)
Google Scholar: [Author Only](#) [Title Only](#) [Author and Title](#)